Results in Engineering 30 (2026) 109938

Contents lists available at ScienceDirect

Results in Engineering

journal homepage: www.sciencedirect.com/journal/results-in-engineering

Research paper

Techno-economic optimization of a hybrid renewable microgrid for electric vehicle charging: A comparative study in Egypt and Türkiye

Ahmad F. Tazay [a], Shimaa Barakat [b], Aykut Fatih Guven [c], Heba I. elkhouly [d], Mohamed Mahmoud Samy [b,e,*]

[a] Electrical Engineering Department, Colleague of Engineering, Al-Baha University, Al Baha, KSA
[b] Department of Electrical Engineering, Beni-Suef University, Beni-Suef, Egypt
[c] Department of Electrical and Electronics Engineering, Faculty of Engineering, Yalova University, Yalova, Turkey
[d] Mechnical Engineering Department, Beni-Suef University, Beni-Suef, Egypt
[e] Department of Electrical and Renewable Energy Engineering, Faculty of Engineering, Nahda University in Beni Suef, Beni Suef, 62764, Egypt

ARTICLE INFO

Keywords:
Hybrid renewable energy microgrid
Electric vehicle charging
Multi-objective optimization
Energy storage systems
Comparative case study

ABSTRACT

The rapid electrification of transport demands EV charging stations supplied by clean, reliable power. This paper presents an optimal sizing framework for an off-grid hybrid renewable microgrid combining photovoltaic arrays, wind turbines, battery energy storage (BESS), and hydrogen energy storage (HESS) to achieve zero loss of power supply probability (LPSP = 0). A four-objective Indicator-Based Evolutionary Algorithm (IBEA) is used to minimize levelized cost of energy (LCOE), curtailment ratio (CR), and LPSP while maximizing renewable fraction (RF). The method is tested in two locations: Attaka, Suez Governorate (Egypt) and Yalova Province (Türkiye), quantifying how climate and finance affect sizing and cost. Türkiye attains a lower LCOE of $0.0173/kWh with RF = 53.03 % and CR = 17.11 %, versus Egypt's $0.0261/kWh, RF = 50.35 %, and CR = 27.67%—a 51.3 % cost advantage driven by balanced solar-wind resources and higher EV demand. Egypt requires substantially larger BESS capacity (227 units vs. 34) to manage solar variability due to its solar-dominant resource profile. Sensitivity analysis reveals that discount and inflation rates dominate LCOE variation (±18–23 % impact), while wind speed and load demand drive operational performance (±15–18% impact). Critical break-even thresholds are 47.5–50 % (Türkiye) and 27.75–30 % (Egypt), indicating Egypt's greater financial fragility. All designs satisfy the strict zero-LPSP constraint (≤0.001 %), confirming the effectiveness of coordinated battery–hydrogen storage for reliable, cost-effective EV charging across diverse climatic and economic contexts.

1. Introduction

The global acceleration of electric vehicle (EV) adoption is placing unprecedented demands on energy infrastructure. Conventional grid-powered charging increases electricity consumption contributes to voltage fluctuations and transformer overloads and perpetuates reliance on fossil fuel-based generation [1,2]. As EV penetration rises, coordinated management of charging loads becomes essential to avoid grid instability [3]. Renewable energy-based microgrids offer a promising localized solution by integrating distributed generation with energy storage and intelligent energy management to serve EV charging loads with substantially reduced emissions and improved energy independence [4,5]. Well-optimized systems have demonstrated renewable fractions exceeding 90 %, LCOE values of $0.02–0.11/kWh, and near-zero loss of power supply probability [6,7]. However, achieving this performance simultaneously across economic, environmental, and reliability dimensions remains a complex multi-objective design problem that is further complicated across diverse geographic and economic contexts.

1.1. Energy storage technologies for EV charging microgrids

PV–wind hybrid systems with appropriately sized storage consistently achieve low LCOE ($0.02–0.08/kWh) and very low LPSP while substantially reducing emissions [8–11]. Storage technology critically determines performance. Battery energy storage systems (BESS) offer high round-trip efficiency and fast response, ideal for intra-day balancing and EV fast-charger buffering but become cost-prohibitive

* Corresponding author at: Faculty of Engineering, Beni-Suef University, Beni-Suef, Egypt.
E-mail address: mohamed.amy@eng.bsu.edu.eg (M.M. Samy).

https://doi.org/10.1016/j.rineng.2026.109938
Received 8 January 2026; Received in revised form 13 February 2026; Accepted 5 March 2026
Available online 8 March 2026

for multi-day autonomy and suffer cycling-dependent degradation [8,12]. Hydrogen energy storage systems (HESS) electrolyzers, tanks, and fuel cells—provide high energy capacity suited for long-duration and seasonal storage but at lower round-trip efficiency and higher capital cost [13,14].

The complementary nature of these technologies is well recognized. In hybrid configurations, batteries handle frequent intra-day fluctuations while hydrogen covers extended low-renewable periods, reducing total system cost relative to single-technology designs [12,15]. Zhang et al. implemented an islanded DC microgrid with both BESS and HESS for an electric-hydrogen hybrid refueling station [16]. Abdelghany et al. coordinated both storage types via model-predictive control in a wind–solar microgrid with EV users [17]. Güven et al. found that PV/wind with both batteries and hydrogen formed the optimal storage backbone for EV charging in Türkiye [7]. Elkholy et al. showed that combined BESS–HESS backup yields the best techno-economic and reliability performance for EV loads in remote microgrids [18]. Despite this progress, joint sizing and operation of BESS and HESS specifically for EV charging microgrids under strict zero-LPSP constraints remains rare. Most zero-LPSP demonstrations target residential or generic loads rather than the high-power, stochastic demand profiles characteristic of EV charging stations [8,19]. Critically, EV-charging cases achieving strict 0 % LPSP rely on batteries and/or grid/diesel backup rather than a true battery–hydrogen hybrid [20,21].

1.2. Multi-objective optimization for microgrid design

Designing EV charging microgrids is inherently multi-objective. NSGA-II dominates the field, applied to campus microgrid sizing [22], hybrid EVCS design [23], and coalition scheduling [24]. Other widely used algorithms include NSGA-III, MOEA/D, MOPSO, and numerous metaheuristics such as IHHO, ISSA, CPSO-ACA, and MOMFA [25–27]. MILP with ε-constraint methods has also been applied for bidirectional EVCS scheduling [28]. Typical objectives include LCOE/TNPC, LPSP, emissions, and power quality metrics [29,30], with constraints on power balance, SOC bounds, and EV arrival patterns [31]. Formal algorithm comparisons using hypervolume, generational distance, and spread metrics are available for this problem class [23,32,33].

Recent research on hydrogen refueling stations (HRS) continues to validate the superiority of hybrid renewable configurations. For instance, Okonkwo utilized HOMER Pro to demonstrate that a PV/Wind hybrid energy system presents the most advantageous techno-economic metrics for a refueling station in Geelong, Australia, achieving an LCOE of $0.4347/kWh. While such studies establish baseline viability, they often rely on single-objective tools, underscoring the need for the multi-objective optimization framework proposed in this study to address more complex trade-offs [34]. However, no study simultaneously treats LCOE, curtailment ratio (CR), renewable fraction (RF), and LPSP as four competing objectives in a single formulation [35,36]. Most include at most two or three, moving others into constraints or post-hoc evaluation. The Indicator-Based Evolutionary Algorithm (IBEA) offers a distinctive approach: it directly optimizes quality indicators—typically hypervolume—providing better Pareto-front convergence on many-objective problems without explicit niching parameters [32].

1.3. Reliability and zero LPSP

For EV charging infrastructure, reliability is a prerequisite for user adoption and commercial viability. Zero LPSP—every unit of demand met at every hour across the full annual cycle—is the appropriate design target. Enforcement typically takes two forms: hard constraint with infeasibility penalty [37,38], or soft objective on a Pareto front from which near-zero solutions are selected [39,40]. Only a small subset of studies verifies strict zero LPSP over a complete 8760-hour simulation: Chen et al. for a standalone PV EVCS, Bilal et al. for a grid-tied PV/wind EVCS, and Sadeghi et al. using MOPSO and NSGA-II for residential microgrids [21,41,42].

The cost implications are significant but manageable. Moving from relaxed reliability (LPSP ≈ 0.05–0.1) toward near-zero typically increases LCOE by 10–20 % in off-grid systems [43,44], though grid-connected systems achieve this at substantially lower premiums [37]. Three critical findings emerge: zero LPSP is rarely enforced as a global hard constraint across the entire optimization [45,46]; among hybrid battery–hydrogen studies, none enforce LPSP = 0 as a hard constraint [47,48]; and EV-charging cases achieving verified 0 % LPSP use battery-only or grid/diesel backup, not hybrid battery–hydrogen storage [20].

1.4. Regional context: Egypt and Türkiye

Optimal microgrid design is inseparable from geographic and economic context. Egypt and Türkiye present an ideal comparative pair for investigating how contrasting renewable resource profiles and EV market maturity interact with similar macroeconomic volatility. The study examines two representative geographic locations: Suez Governorate, Attaka, Egypt (29°40.3′N, 32°20.1′E) and Yalova Province, Türkiye (40°39.1′N, 29°13.2′E). The Egyptian site, located along the Suez–Ain El Sokhna Road, represents an emerging EV charging infrastructure corridor in an industrial transitional zone. The Turkish site at Yalova University Central Campus situates the analysis within the high-EV-potential Istanbul–Bursa metropolitan corridor.

Egypt is a solar-dominant developing economy with annual solar irradiance of 3.0–8.15 kWh/m^2/day, moderate wind speeds of 5.1–5.9 m/s, a nascent EV market [49,50], and high macroeconomic volatility (35 % nominal interest rate, 34 % inflation). Egypt targets 42 % renewable energy by 2030. Türkiye offers a diversified renewable portfolio—solar capacity doubled to 19.6 GW by end of 2024, with a 120 GW wind-solar target by 2035—a more developed EV market, and similarly volatile macroeconomic conditions (47.5 % interest rate, 47.09 % inflation). These contrasting conditions—Egypt's solar-centric resource dependency versus Türkiye's balanced renewable mix, coupled with Egypt's emerging versus Türkiye's mature EV adoption—create a natural experimental framework for sensitivity analysis while shared macroeconomic volatility ensures economic parameter comparability. While recent studies have made significant strides in the frequency control and stability of diesel-integrated microgrids in Egypt using Adaptive and Fuzzy PI controllers [51,52], there remains a gap in the techno-economic optimization of fully renewable (diesel-free) systems that integrate hybrid hydrogen storage for stochastic loads.

Existing Türkiye-linked work includes Güven et al., who optimized hybrid systems for EV charging in the Çukurova region. Egypt-linked work includes Hassan, who simulated a hydrogen microgrid in Aswan for general loads, not EV charging [5,53]. However, no published study optimizes EV-focused charging microgrids with integrated hydrogen storage across these two countries using a unified methodology, nor does comparable work examine cross-regional sensitivity to financial and operational parameters. No study presents a techno-economic optimization of an EV-focused charging microgrid with hydrogen storage compared across Egypt and Türkiye. More broadly, cross-country comparative studies of EV charging microgrids are virtually absent from the literature; existing comparisons are multi-site within single countries [54–56]. Sensitivity analyses show that financial parameters (discount and inflation rates) and operational parameters (wind speed, solar irradiance) drive cost and performance variation [57,58], yet cross-regional comparative sensitivity analysis remains a notable void.

1.5. Comparison with state-of-the-art studies

Table 1 positions this work within the recent literature (2021–2025).

No existing study simultaneously optimizes LCOE, CR, RF, and LPSP using a formal multi-objective algorithm with hybrid battery–hydrogen storage across multiple countries. IBEA has not applied to this domain.

Table 1
Comparative summary of state-of-the-art studies on renewable microgrid optimization for EV charging (2021–2025).

Year	Study Region	Optimization Algorithm	System Configuration	Financial Viability Metrics	Main Results	Limitations	Refs.
2025	Çukurova, Türkiye	HOMER	PV/WT/Biomass/H_2/Grid	LCOE, NPC	LCOE = \$0.0215/kWh; high self-sufficiency with PV + biomass + H_2 + grid	Single region; no multi-objective optimization; no LPSP enforcement; HOMER-based tool only	[5]
2025	NEOM, Saudi Arabia	HOMER	PV/WT/BESS/H_2 (3 configurations)	NPC, LCOE, LPSP	Hybrid BESS–H_2 improves energy dependability vs. battery-only at somewhat higher NPC	Single site; no EV-specific stochastic load model; LPSP evaluated post-hoc, not enforced as hard constraint	[13]
2024	Island and urban networks	MMOSSA	PV/WT/BESS-VSG + EVCS	TNPC, LCOE, CO_2	LCOE ≈ \$0.038–0.047/kWh; ~89 % CO_2 reduction vs. reference case	No hydrogen storage; LPSP used in numerical comparison, not as optimization constraint; single-country scope	[4]
2024	Generic (hotel + EVCS)	QIBWO	PV/WT/BESS + Hotel + EVCS	LCOE, LPSP	LCOE = \$0.053/kWh; LPSP ≈ 0.001 %; RF = 95.8 %	No hydrogen storage; single site; no curtailment ratio optimization; no regional comparison	[7]
2024	Saudi Arabia (EV charging)	NSGA-II, NSGA-III, MOEA/D, MOPSO	PV/WT/BESS + EVCS	TNPC, LPSP	NSGA-II achieves best convergence and diversity; near-zero LPSP on Pareto front	Battery-only storage; bi-objective formulation (TNPC vs. LPSP); no CR or RF as objectives; no cross-regional analysis	[40]
2024	India (grid-tied EVCS)	POA and metaheuristics	PV/WT/Grid + EVCS	TNPC, LCOE, LPSP	LPSP swept from 0 % to 5 %; LCOE = \$0.038–0.08/kWh across configurations	Grid-tied with no hydrogen storage; LPSP treated as parametric sweep, not hard constraint; single country	[59]
2025	Generic (standalone EV)	CPSO-ACA	PV/WT/FC (standalone)	NPC, LCOE, LOLP, LOLE, LOEE	Standalone system with fuel cell serves stochastic EV load; reliability via LOLP indices	No battery–hydrogen co-optimization; reliability via LOLP family, not explicit LPSP = 0; no regional comparison	[26]
2024	United Kingdom	Custom simulator	PV/WT/Hybrid BESS (Li-ion, LA, 2nd-life)	MCOE, NPC	Second-life Li-ion gives lowest total cost; hybrid BESS deepens usable DoD	No hydrogen storage; no EV-specific stochastic charging model; single region; no multi-objective framework	[6]
2024	United Kingdom	MILP	PV/WT/Hybrid BESS	NPC, EENS	Hybrid BESS cuts storage cost 4.6–21 % vs. single battery technologies; ageing deferred	Battery-only (no hydrogen); EV load profiles simplified; single-region analysis	[8]
2024	Remote area	Comparative analysis	PV/WT/BESS/HESS/EVB (V2G)	TNPC, LCOE	Combined BESS–HESS–EVB backup gives best techno-economic and reliability performance for EV loads	No formal multi-objective optimization; no LPSP = 0 enforcement as hard constraint; single site	[18]
2025	Generic distribution grid	Multi-objective scheduling	RES/H_2 storage + EV charging + H_2 stations	Cost, losses, emissions, voltage security	Multi-service hydrogen scheduling for battery-EV and fuel-cell-EV stations	No cross-regional comparison; LPSP not explicitly constrained; no sensitivity to macroeconomic parameters	[60]
2024	Malaysia (multiple locations)	HOMER	PV/WT/BESS/H_2/Grid + EVCS	NPC, LCOE, CO_2	Hydrogen storage integrated with grid-connected EV charging; location-dependent optimal mixes	HOMER-based single-objective tool; single country; no formal multi-objective optimization; no LPSP enforcement	[61]
2025	New Administrative Capital, Egypt	HOMER	PV/WT/DG/BESS/FC/ELZ/HT	NPC, LCOE, RF	Islanded AC microgrid with full PV-WT-DG-BESS-FC-ELZ-HT hybrid configuration	Includes diesel generator (not fully renewable); general school load, no EV-specific demand; single site; no multi-objective optimization	[62]
2026	**Egypt & Türkiye (comparative)**	**IBEA (4-objective)**	**PV/WT/BESS/ELZ/FC/H_2T (no diesel)**	**LCOE, CR, RF, LPSP**	**Egypt: LCOE = \$0.0261/kWh, RF = 50.35 %, CR = 27.67 %, LPSP = 0; Türkiye: LCOE = \$0.0173/kWh, RF = 53.03 %, CR = 17.11 %, LPSP = 0**	**Assumes perfect component availability; single-year climate data; rule-based EMS**	**This study**

The present study addresses all these gaps.

1.6. Research gaps, objectives, and contributions

The preceding analysis reveals six interrelated gaps:

- **Gap 1.** No study simultaneously optimizes LCOE, CR, RF, and LPSP as four competing objectives for EV charging microgrids.
- **Gap 2.** Zero LPSP is rarely enforced as a hard constraint; among hybrid battery–hydrogen studies, none impose strict LPSP = 0 for EV charging.
- **Gap 3.** Hybrid battery–hydrogen storage co-optimized for stochastic EV charging demand under strict reliability constraints remains largely unexplored.
- **Gap 4.** No cross-country comparative analysis of EV charging microgrids exists using a unified optimization framework.
- **Gap 5.** IBEA has not been applied to EV charging microgrid optimization.
- **Gap 6.** Cross-regional sensitivity analysis comparing how identical designs respond to contrasting macroeconomic environments is.

The research objectives and corresponding contributions are:

- Develop a four-objective IBEA optimization framework (LCOE, CR, RF, LPSP) with zero-LPSP as a hard constraint using hybrid battery–hydrogen storage for EV charging (Gaps 1, 2, 3, 5).
- Design a rule-based EMS with AC/DC load prioritization and load shifting tailored to stochastic EV charging demand (Gap 3).

- Conduct the first comparative Egypt–Türkiye analysis of EV charging microgrids using a unified methodology (Gap 4).
- Perform comprehensive cross-regional sensitivity and break-even analysis across financial and operational parameters (Gap 6).

2. Methodology

This section presents the methodological framework for the effective design, functioning, and efficiency of the hybrid renewable energy microgrid, considering the main objectives—namely LCOE and LPSP or CR minimization while increasing RF. The main goals in optimizing renewable energy modeling are surplus and deficit power management, dynamic load priority management, and multi-objective optimization using a meta-heuristic IBEA.

2.1. System modeling

The proposed microgrid system integrates solar photovoltaic panels, wind turbines, battery energy storage systems, hydrogen storage units, and electric vehicle supply equipment to sustain electric vehicles in residential communities. Fig. 1 illustrates the architecture of the system. In this simulation, an hourly time resolution over a one-year horizon is assumed, which presents a good balance between computational efficiency and temporal granularity. This resolution captures the diurnal variations in renewable energy generation, demand patterns, and storage dynamics while offering an accurate representation of system performance for a wide range of operational scenarios with manageable computational complexity.

2.1.1. Battery energy balance

The battery's state of charge (SOC) is updated at every step based on charging and discharging operations:

Battery Charging Model:

$$SOC(t) = SOC(t-1) + \frac{P_{\text{bat, charge}}(t)\cdot\eta_{\text{bat}}\cdot\Delta t}{E_{\text{bat}}} \quad (1)$$

Battery Discharging Model:

$$SOC(t) = SOC(t-1) - \frac{P_{\text{bat, discharge}}(t)\cdot\Delta t}{E_{\text{bat}}\cdot\eta_{\text{bat}}} \quad (2)$$

The battery SOC is constrained as follows:

$$SOC_{\min} \le SOC_t \le SOC_{\max}$$

where:

- $\boldsymbol{SOC(t)}$= State of Charge at time t (%)
- $\boldsymbol{P_{bat,charge}(t)}$= Battery charging power at time t (kW)
- $\boldsymbol{P_{bat,discharge}(t)}$= Battery discharging power at time t (kW)
- $\boldsymbol{\eta_{bat}}$= Battery round-trip efficiency (0.97 for Li-ion; unitless)
- $\boldsymbol{E_{bat}}$= Total battery capacity (kWh)
- $\boldsymbol{\Delta t}$= Time step (1 hour)
- $\boldsymbol{SOC_{min}, SOC_{max}}$= Minimum and maximum SOC constraints (set to 20 % and 95 %, respectively, to preserve battery lifespan)

2.1.2. Hydrogen tank dynamics

The hydrogen tank serves as long-term energy storage, converting surplus electricity into hydrogen via electrolysis and utilizing hydrogen fuel cells for electricity generation during periods of energy deficit. This section details the mathematical model governing the system's hydrogen production, storage, and consumption.

Electrolyzer Operation:

$$H_{2produced}(t) = \frac{P_{\text{el}}(t)\cdot\eta_{\text{el}}}{HHV}\ .\ \Delta t \quad (3)$$

Where:

- $\boldsymbol{H_{2produced}(t)}$= Hydrogen production rate at time t (kg/h)
- $\boldsymbol{P_{el}(t)}$= Electrolyzer input power at time t (kW)
- $\boldsymbol{\eta_{el}}$= Electrolyzer efficiency (0.85; unitless)
- $\boldsymbol{HHV}$ = Higher Heating Value of hydrogen (39.4 kWh/kg)

Fuel Cell Operation:

The fuel cell power output is constrained by both its maximum capacity and the available hydrogen:

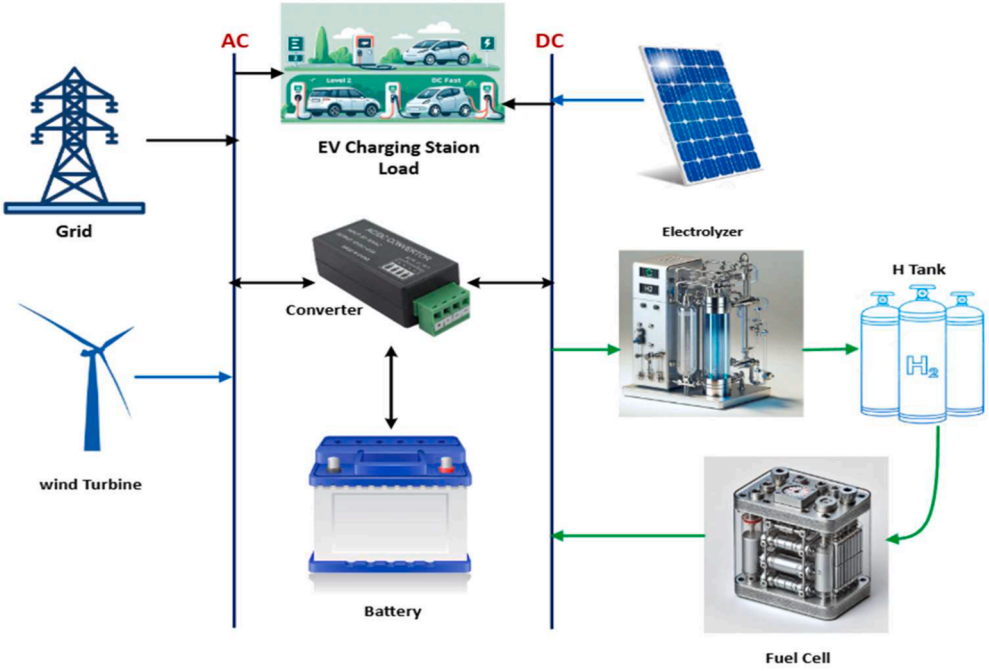

Fig. 1. Hybrid renewable microgrid system architecture.

$$P_{fc}(t) = \min\left(P_{fc,\ max}, \frac{H_{tank}(t)\cdot HHV\cdot\eta_{fc}}{\Delta t}\right) \quad (4)$$

where:

- $P_{fc}(t)$= Fuel cell power output at time t (kW)
- $P_{fc,max}$= Maximum fuel cell rated power (kW)
- $H_{tank}(t)$= Hydrogen stored in tank at time t (kg)
- η_{fc}= Fuel cell efficiency (0.60; unitless)

Hydrogen Consumption:

The hydrogen consumed by the fuel cell is calculated based on the power output, efficiency, and energy content:

$$\Delta H_{2consumed}(t) = \frac{P_{fc}(t)\cdot\Delta t}{HHV\cdot\eta_{fc}} \quad (5)$$

Hydrogen Tank State:

The hydrogen tank state is updated by accounting for the hydrogen produced and consumed during each time step:

$$H_{tank}(t) = H_{tank}(t-1) + H_{2produced}(t) - \Delta H_{2consumed}(t) \quad (6)$$

Hydrogen storage is subject to the following constraints to ensure safe and efficient operation:

$$H_{\min} \le H_{tank}(t) \le H_{\max}$$

where:

- H_{min}, H_{max}= Minimum and maximum hydrogen tank storage capacity constraints (kg)
- H_{min} is set to 10 % of H_max to maintain system responsiveness
- H_{max} is optimized as a decision variable in the IBEA framework

This integrated system dynamically manages energy across multiple storage and generation subsystems, optimizing efficiency and operational resilience. The hydrogen subsystem specifically addresses the needs for long-duration energy storage, complementing the battery storage system, which is faster responding but capacity-limited, to ensure a reliable power supply under all operating conditions.

2.2. Renewable energy generation modeling

2.2.1. Photovoltaic (PV) power generation

The PV power output is a crucial system element, and its performance is modeled using the following equation. The hourly PV power output is determined based on solar irradiance data utilizing a modified one-diode model:

$$P_{\mathrm{PV}}(t) = P_{\mathrm{rated,PV}}\cdot N_{\mathrm{PV}}\cdot f_{\mathrm{df}}\cdot G_t(\mathrm{t})\cdot\left[1 + K_t\cdot\left(T_{c,t} - T_{\mathrm{ref}}\right)\right] \quad (7)$$

where:

- $P_{PV}(t)$= Photovoltaic power output at time t (kW)
- N_{PV}= Number of PV panels (decision variable; unitless)
- $P_{rated,PV}$= Rated power of single PV panel (5 kW per unit)
- f_{df}= PV derating factor accounting for soiling, mismatch losses, and wiring losses (0.8; unitless)
- $G_t(t)$= Solar irradiance at time t (kWh/m^2/day)
- G_{ref}= Reference solar irradiance (1 kWh/m^2/day)
- K_t= Temperature coefficient of performance (−0.005/°C)
- $T_c(t)$= PV cell temperature at time t (°C), calculated as:

$$T_c(t) = T_a(t) + \frac{G_t(t)}{1000}\,(NOCT - 20)$$

where $T_a(t)$ is ambient temperature and NOCT is the Nominal Operating Cell Temperature (47°C for standard modules).

- T_{ref} = Reference cell temperature (25°C)

This equation models the conversion of solar irradiance into electrical energy, a fundamental aspect of cleaner energy generation. The model incorporates cell temperature dynamics through the NOCT-based approach, ensuring accurate representation of PV performance across the seasonal temperature variations observed in both Egypt and Türkiye (Figs. 7 and 10).

2.2.2. Wind turbine (WT) power generation

Wind energy generation is modeled using the following piecewise function. The hourly WT power output, denoted as (P_WT(t)), is modeled by:

$$P_{WT}(t) = \begin{cases} 0 & v_{ci} \ge v(t) \ge v_{co} \\ N_{WT}\ .\ P_{WT_{rated,WT}}\cdot\dfrac{v(t)^3 - v_{ci}^3}{v_r^3 - v_{ci}^3} & v_{ci} \le v(t) \le v_r \\ N_{WT}\ .\ P_{WT_{rated,WT}} & v_r \le v(t) \le v_{co} \end{cases} \quad (8)$$

where:

- $P_{WT}(t)$= Wind turbine power output at time t (kW)
- N_{WT}= Number of wind turbines (decision variable; unitless)
- $P_{rated,WT}$= Rated power of single wind turbine (100 kW per turbine)
- $v(t)$= Wind speed at time t (m/s)
- v_{ci}= Cut-in wind speed (3 m/s)
- v_{co}= Cut-out wind speed (25 m/s)
- v_r= Rated wind speed (12 m/s)

This model captures the operational thresholds and power output across varying wind regimes, with air density correction optionally applied for high-altitude sites. The piecewise formulation reflects the characteristic power curve of horizontal-axis wind turbines, ensuring realistic representation across the consistent wind speed ranges observed in both study locations (Fig. 6 and 9). Air density correction for high-altitude sites is not applied, as both Egypt (Suez, 29°40.3′N, 32°20.1′E) and Türkiye (Yalova, 40°39.1′N, 29°13.2′E) are at low elevations with standard sea-level air density (~1.225 kg/m^3).

2.3. EV Charging station model

This section formalizes the mathematical representation of EV charging station loads by incorporating vehicle properties, charging preferences, environmental factors, and load prioritization strategies. The model integrates probabilistic approaches, dynamic time-based arrival patterns, non-linear charging behavior, and ecological effects to analyze EV charging station operations comprehensively.

2.3.1. Model assumptions

The following assumptions underpin the model:

1. All chargers are equally available and fully operational throughout the simulation.
2. Vehicle arrivals follow Poisson distribution and are assumed to be independent of each other.
3. Users select chargers based on a probabilistic model influenced by time of day and vehicle capabilities.
4. Weather, temperature, and grid fluctuations affect the load profile probabilistically.
5. Vehicles aim to reach a target SOC between 85–95 %.
6. Once assigned, a vehicle remains on the same charger until charging is complete.

2.3.2. Vehicle properties

Vehicle properties are characterized probabilistically to reflect fleet diversity:

Battery Capacity Distribution:

Battery capacity follows a normal distribution, reflecting variability from manufacturing processes and battery aging effects:

$$\mu_{C_b} \sim \mathcal{N}\left(\overline{\mu}_{C_b}, \sigma^2_{C_b}\right) \tag{9}$$

This assumption aligns with the Central Limit Theorem, as multiple independent factors influence battery capacity [63,64]. Capacity varies by vehicle type and regional fleet composition.

Maximum Charging Rate Distribution:

The maximum charging rate is modeled using a truncated normal distribution, ensuring values remain within realistic operational limits:

$$\mu_{\mathrm{P_{max}}} \sim \mathcal{N}_{trunc}\left(\overline{\mu}_{\mathrm{P_{max}}}, \sigma^2_{P_{max}}, \mathrm{P_{min}}, \mathrm{P_{max}}\right) \tag{10}$$

Truncation bounds ($P_{min} = 1kW, P_{max} = charger\ power\ rating$) ensure realistic values.

Initial and Target State of Charge:

The initial SOC follows a uniform distribution, reflecting the variability in user behavior:

$$SOC_i \sim U(SOC_{min}, SOC_{max}) \tag{11}$$

User-defined target SOC varies probabilistically:

$$SOC_t = 85 + 10 \cdot \xi, \quad \xi \sim U(0,1) \tag{12}$$

Initial SOC reflects typical arriving vehicle conditions. Target SOC reflects user preference for adequate range without full charging (reducing time and degradation).

Energy Required and Charging Duration:

The energy required to charge from initial SOC to target SOC is:

$$E_{required} = \frac{SOC_t - SOC_i}{100} \times \mu_{C_b} \tag{13}$$

Charging Power (P_{charge})

The charging power depends non-linearly on SOC:

$$P_{charge} = P_{max} \cdot f_{curve}(SOC) \tag{14}$$

Charging duration is calculated as:

$$t_c = \frac{E_{required}}{P_{avg}} [minutes] \tag{15}$$

where P_{avg} is the average charging power accounting for power tapering across the SOC range.

2.3.3. Vehicle arrival model

Vehicle arrivals follow a non-homogeneous Poisson process, reflecting time-of-day variations:

$$\lambda(h) = \lambda_{base} \cdot f_{time}(h) \tag{16}$$

Time-of-Day Factor:

The time-of-day factor adjusts arrival rates based on typical commuting patterns. For weekdays, the factor is modeled as:

$$f_{\mathrm{time}}(h) = \begin{cases} 0.25 & h \in [1,5)\ \text{(night)} \\ 1.50 & h \in [7,9)\ \text{(morning peak)} \\ 0.80 & h \in [10,14)\ \text{(midday)} \\ 1.80 & h \in [16,20)\ \text{(evening peak)} \\ 0.50 & h \in [21,24)\ \text{(late evening)} \end{cases} \tag{17}$$

On weekends, the arrival rate is scaled:

$$\lambda_{weekend} = 0.65 \times \lambda_{weekday}(h) \tag{18}$$

2.3.4. Charger assignment and queue management

Assignment Algorithm: When a vehicle arrives, the system attempts assignment to an available charger of the requested type. If no chargers are available, the vehicle enters a queue.

Queue Processing: At each time step, queued vehicles are assigned to chargers as they become available (FIFO discipline). Queue length and wait time statistics are recorded for each charger type:

$$queueLength(t) = numberofvehicleswaiting \tag{19}$$

$$chargerUtilization(t) = \frac{active\ chargers}{total\ chargers} \tag{20}$$

2.3.5. Hourly load aggregation and environmental adjustments

The total hourly load aggregates active charging sessions:

$$P_{hour} = \sum_{sessions\ in\ hour\ h} P_{charge}(t) \tag{21}$$

Load is aggregated at 1-minute resolution across 525,600 minutes (annual simulation) and accumulated into 24-hour bins.

Environmental Adjustments:

$$P_{\mathrm{adjusted}}(h) = P_{\mathrm{hour}}(\mathrm{h}) \cdot f_{\mathrm{temp}}(h) \cdot f_{\mathrm{weather}}(h) \cdot f_{\mathrm{grid}}(h) \tag{22}$$

where:

$$f_{temp}(t) = 1 + 0.02 \times (T(h) - 25^{\circ}C) \tag{23}$$

$T(t)$ is the ambient temperature at time t (°C)

$$f_{\mathrm{weather}}(t) = 1 + X(h).\sigma_{\mathrm{weather}} \tag{24}$$

$$f_{\mathrm{grid}}(t) = 1 + Y(h).\sigma_{\mathrm{grid}} \tag{25}$$

$X(h), Y(h) \sim U(-0.1, 0.1)$ represent stochastic variations; $\sigma_{weather}, \sigma_{grid} \approx 0.05 - 0.10$ allow ±5–10 % load variation due to environmental and grid conditions. Temperature adjustment accounts for reduced charging efficiency in cold climates (2 % per°C below 25°C) and reflects the seasonal temperature variations shown in Figs. 7 and 10.

2.4. Energy management flow

The Energy Management Flow (EMF) serves as the operational backbone of the hybrid renewable energy microgrid, ensuring efficient utilization of available energy resources, minimizing operational costs, and maintaining system reliability under fluctuating energy generation and demand conditions. The EMF dynamically manages the interactions among PV panels, wind turbines, battery energy storage systems (BESS), hydrogen storage systems, fuel cells, and grid interactions. The EMF balances short-term operational responses with long-term strategic goals while operating at an hourly temporal resolution over a one-year simulation horizon (8,760 hours). The EMF framework consists of four main functional strategies:

- Renewable Energy Allocation
- Surplus Energy Management
- Deficit Energy Management
- Load Shifting and Shedding Mechanisms

These strategies operate sequentially based on a rule-based priority system that is executed at each hourly time step. The core logic is designed to handle two primary scenarios: the management of an energy surplus, where renewable generation exceeds load demand, and the management of an energy deficit, where loads surpass available renewable power. The complete sequential logic of the EMS is visually detailed in the flowchart presented in Fig. 2. This flowchart illustrates the decision-making process at each time step, from calculating the initial net power balance to the prioritized allocation of resources for

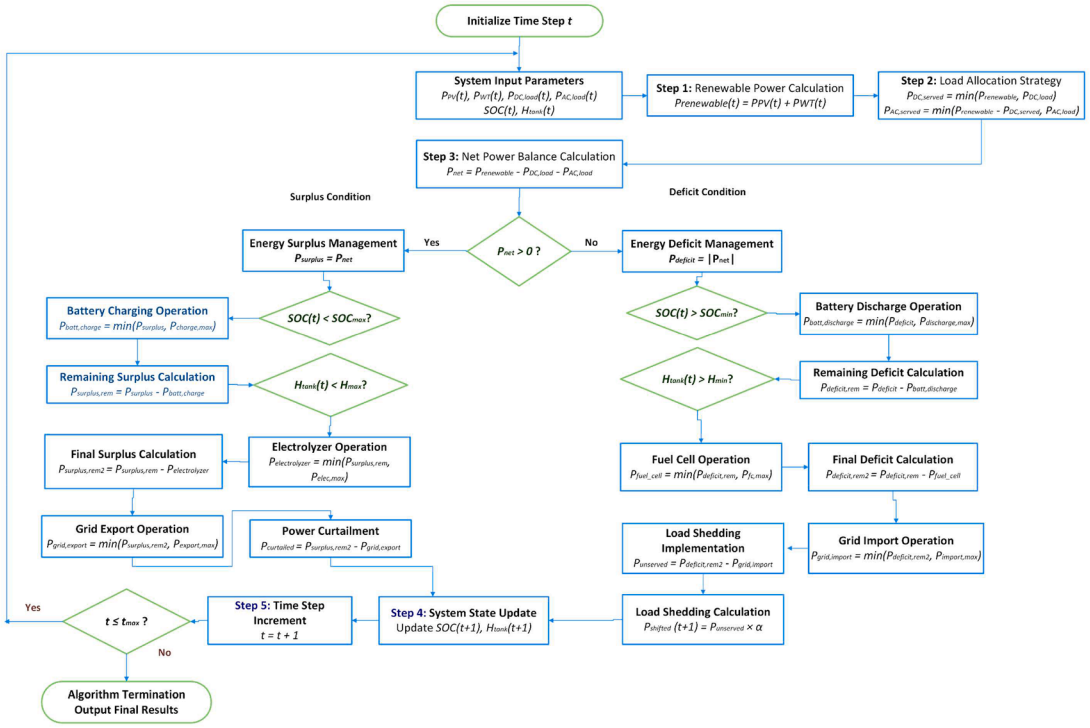

Fig. 2. Sequential logic flowchart of the rule-based energy management system (EMS).

battery charging, hydrogen production, grid interaction, and, when necessary, load management.

2.4.1. Renewable energy allocation

Renewable energy from PV panels and wind turbines is allocated at each time step to meet the demands of Direct Current (DC) loads (critical infrastructure, EV fast-charging) and Alternating Current (AC) loads (EV Level 2, residential/commercial), prioritizing DC loads but enabling simultaneous fulfillment if sufficient energy exists; this allocation is mathematically expressed as:

1. DC Load Fulfillment:

$$P_{DC}(t) = \min\left(P_{renewable}(t), P_{DC\_load}(t)\right) \tag{26}$$

2. AC Load Fulfillment:

$$P_{AC}(t) = \min\left(P_{renewable}(t) - P_{DC}(t), P_{AC\_load}(t)\right) \tag{27}$$

Any remaining renewable energy after fulfilling both loads is classified as surplus energy and managed according to the surplus management strategy.

2.4.2. Surplus energy management

Surplus energy arises when renewable generation exceeds the combined DC and AC load demands. The EMS prioritizes surplus distribution as follows:

1. Battery Charging:

$$P_{surplus}(t) = P_{renewable}(t) - P_{DC}(t) - P_{AC}(t) \tag{28}$$

If $P_{surplus}(t) > 0$ and $SOC(t) < SOC_{max}$:

$$P_{battery_charge}(t) = \min\left(P_{surplus}(t),\ P_{batery_max},\ E_{battery} - SOC(t)\right) \tag{29}$$

2. Hydrogen Production via Electrolyzer:

The remaining surplus energy is directed to electrolyzers for hydrogen production:

$$P_{remaining}(t) = P_{surplus}(t) - P_{battery_charge}(t) \tag{30}$$

The power directed to the electrolyzer is determined based on the residual surplus energy:

$$P_{electrolyzer}(t) = min\left(P_{remaining}(t), P_{electrolyzer,max}(t)\right) \tag{31}$$

3. Grid Export:

If both battery and hydrogen storage capacities are saturated, excess energy is exported to the grid:

$$P_{grid\_export}(t) = \max\left(0,\ P_{remaining}(t) - P_{electrolyzer}(t)\ - P_{grid\_export\_max}\right) \tag{32}$$

4. Curtailment:

Remaining energy that cannot be utilized or exported is curtailed:

$$P_{curtailed}(t) = max\left(0, P_{grid\_export}(t) -\ P_{grid\_export\_max}\right) \tag{33}$$

2.4.3. Deficit energy management

Deficit energy occurs when renewable energy generation is insufficient to meet load demand. Deficit energy is managed sequentially through the following steps:

1. Battery Discharging:

$$P_{deficit}(t) = P_{DC}(t) + P_{AC}(t) - P_{renewable}(t) \tag{34}$$

If $P_{deficit}(t) > 0$ and $SOC(t) > SOC_{min}$:

$$P_{battery\_discharge}(t) = \min\left(P_{deficit}(t), P_{batery_{max}},\ SOC(t).E_{battery}\right) \quad (35)$$

2. Hydrogen Fuel Cell Operation:

$$P_{remaining_{dici}}(t) = P_{deficit}(t) - P_{battery\_discharge}(t) \quad (36)$$

If $P_{remaining_{dici}}(t) > 0$ and $H_{tank}(t) > H_{min}$:

$$P_{fuelcell}(t) = \min\left(P_{remaining_{dici}}(t), P_{fc\_max}(t), \frac{H_{tank}(t).HHV.\eta_{fc}}{\Delta t}\right) \quad (37)$$

3. Grid Import:

$$P_{remaining_{dici}}(t) = P_{deficit}(t) - P_{battery\_discharge}(t) - P_{fuelcell}(t) \quad (38)$$

If $P_{remaining_{dici}}(t) > 0$ and grid is available:

$$P_{grid\_import}(t) = \min\left(P_{remaining_{dici}}(t), P_{grid\_import\_max}\right) \quad (39)$$

4. Load Shedding:

$$P_{unserved}(t) = max\left(0, P_{deficit}(t) - P_{battery.discharge}(t) - P_{fuelcell}(t) - P_{grid.import}(t)\right) \quad (40)$$

2.4.4. Load shifting mechanism

Non-critical loads are dynamically shifted to periods with higher renewable availability:

$$P_{shifted}(t+1) = \alpha.\ P_{unserved}(t) \quad (41)$$

Where:

- α = Load shift efficiency factor (0.8–0.95; accounts for losses during shifting).
- $P_{shifted}(t+1)$ = Load shifted power in the next time step (kW).

The load shifting mechanism attempts to reschedule a portion of unserved EV charging loads to subsequent hours when renewable generation is expected to be higher, based on historical patterns and weather forecasts. This is particularly effective for flexible loads (Level 2 EV chargers) with extended charging windows.

2.5. Multi-objective optimization framework with IBEA

Balancing four conflicting objectives—minimizing the LCOE, LPSP, and CR while maximizing the RF—is central to the optimization of a hybrid renewable energy microgrid. This study introduces an advanced framework leveraging the IBEA as its core optimization engine. The IBEA integrates hypervolume metrics and adaptive mutation mechanisms to achieve Pareto-optimal solutions, offering a robust approach for addressing multi-objective challenges. This section introduces the key objectives, followed by a detailed discussion of the algorithm, decision variables, objective functions, constraints, and implementation methodology, focusing on the synergy between IBEA and the Energy Management System (EMS).

2.5.1. Indicator-based evolutionary algorithm (IBEA)

IBEA was chosen for its distinctive ability to address conflicting objectives effectively through hypervolume-based fitness assignment, which directly measures the quality of the Pareto front rather than relying on explicit niching parameters. Unlike NSGA-II, which uses crowding distance and rank-based selection, IBEA optimizes the hypervolume metric directly, providing superior performance on many-objective problems (3+ objectives). This is particularly advantageous for the four-objective optimization (LCOE, CR, RF, LPSP) formulated in this study.

To implement the algorithm for this study, the control parameters detailed in Table 2 were selected based on common practices in the literature for complex engineering optimization problems and were refined through preliminary experiments to ensure stable convergence.

2.5.1.1. Hypervolume metric for fitness assignment. The hypervolume metric evaluates solution quality by measuring the volume of the objective space dominated by a solution relative to a reference point. Key features include:

Assigning fitness based on a solution's contribution to the overall hypervolume.
Prioritizing solutions that dominate larger areas in the objective space during selection and filtering.

The hypervolume is mathematically expressed as:

$$HV = \int_R 1_{\{f(x)\ \ dominates\ \ r\}}\ d\boldsymbol{r} \quad (42)$$

Where:

- $f(x)$ = Objective vector $\left[f_1(x), f_2(x), f_3(x), f_4(x)\right]$ corresponding to [LCOE, LPSP, CR, RF]
- $\boldsymbol{r}$: Reference point in the objective space.
- $1_{\{\}}$: The indicator function returns to one if a solution dominates the point and zero otherwise.

Reference Point for Hypervolume:

The reference point is derived from the worst-case values observed in the objective functions during initial population generation. A small positive margin (ε) ensures the reference point is outside the dominated region, enhancing exploration and preventing convergence to local optima. It is mathematically defined as:

$$\mathbf{r} = \left(\text{worst}(f_1) + \varepsilon_1, \left|\text{worst}(f_2) + \varepsilon_2, \right|\text{worst}(f_3) + \varepsilon_3, \left|\text{worst}(f_4) - \varepsilon\right.\right. \quad (43)$$

Where: where $\varepsilon = 0.01\ \times range(f_i)$ for each objective i, ensuring the reference point is slightly beyond the worst observed values (for minimization objectives 1–3) and below the best observed value (for maximization objective 4, RF).

2.5.1.2. Adaptive mutation mechanisms. Mutation diversifies the population and mitigates premature convergence. The mutation rate (μ) is dynamically adjusted based on algorithmic convergence. The fitness is calculated with LCOE priority:

Table 2
IBEA Parameter values.

Parameter	Value	Description	Refs.
Population Size (Npop)	100	Number of individuals in the population.	[65]
Maximum Generations (Ngen)	50	Maximum number of iterations.	[66]
Crossover Index (ηc)	20	Distribution index for crossover.	[67]
Mutation Rate (μ)	0.1	Initial mutation rate.	[67]
Mutation Step Size (σ)	0.2	Step size for Gaussian mutation.	[68]
Adaptation factor (α)	0.8	Typically, between 0.8 and 1.2.	[69]
η_c	20	Distribution index for SBX crossover	[67]

$$Fitness(i) = -\text{Cost}(i,1) + \sum_{j \neq i} \text{indicatorFunction}(\text{Cost}(j), \text{Cost}(i)) \quad (44)$$

where the negative LCOE term provides priority toward economic objectives, and the indicator function sum captures multi-objective dominance relationships. This hybrid approach balances LCOE minimization with multi-objective Pareto optimality.

The adaptive mutation mechanism operates as follows:

$$\mu(g) = \begin{cases} \min(\mu(g-1)/0.95, \mu_{\max}) & \text{if } \Delta HV(g) < \Delta HV_{\min} \text{ (stalling)} \\ \max(\mu(g-1) \times\ 0.95, \mu_{\min}) & \text{if } \Delta HV(g) > \Delta HV_{\max} \text{ (improving)} \end{cases} \quad (45)$$

where:

- $\Delta HV(g)$ = Change in hypervolume from generation $g-1$ to g
- $\mu_{\min} = 0.001$, $\mu_{\max} = 0.2$
- Adaptation factor $= 0.95$

If successive generations show little to no improvement in hypervolume, the mutation rate increases to explore new search space regions. Conversely, if significant progress is observed, the mutation rate is decreased to focus on fine-tuning solutions. These adaptive mechanisms ensure the search process remains efficient and responsive to the optimization landscape.

2.5.2. Decision variables

The decision variables, carefully selected based on their critical role in influencing microgrid performance, represent controllable system parameters. These include:

- N_{PV}: Number of photovoltaic (PV) panels.
- N_{WT}: Number of wind turbines.
- N_{BAT}: Number of battery storage units.

The bounds for these variables are:

$$N_{PV} \in [0, 200],\ N_{WT} \in [0, 20],\ N_{BAT} \in [0,\ 400]$$

These decision variables are optimized via IBEA to minimize LCOE while satisfying zero-LPSP constraint. The electrolyzer (Ele_N), fuel cell (FC_N), and hydrogen tank ($H2T_N$) capacities are implicitly determined from the energy balance requirements and surplus/deficit management strategy, rather than being direct decision variables. This reduces problem dimensionality while maintaining system flexibility.

2.5.3. Objective functions

The optimization process focuses on four key objectives, evaluated hourly across a year-long time horizon (T = 8760 hours). These objectives frequently interact and may conflict, requiring a balanced approach. The multi-objective optimization problem can be expressed as:

$$minimize/\ maximize F(x) = \left[f_1(x), f_2(x), f_3(x), f_4(x)\right] \quad (46)$$

1. Minimization of Levelized Cost of Energy (LCOE):

The LCOE represents the average cost of electricity generation over the system's lifetime, incorporating initial capital costs, operational and maintenance costs, replacement costs, and salvage values.

$$f_1(x) = LCOE = \frac{Net\ Annual\ Cost}{Total\ Energy\ Served} \quad (47)$$

where:

$$\text{Net Annual Cost} = (\text{Total Annualized Cost}) - (\text{Annual Revenue}) \quad (48)$$

$$\text{Total Annualized Cost} = \sum_{i \in \text{components}} \left[C_{\text{cap},i} \cdot CRF + C_{\text{O\&M},i} + \frac{C_{\text{repl},i}}{(1+r)^{t_{\text{repl}}}} - \frac{S_i}{(1+r)^N} \right] \quad (49)$$

$$CRF = \frac{r(1+r)^N}{(1+r)^N - 1} \quad (50)$$

Where:

- $C_{\text{cap},i}$ (USD): Initial capital cost of component i.
- $C_{\text{OM},i}$ (USD/year): Annual operation and maintenance costs of component i.
- $C_{\text{repl},i}$ (USD): Replacement cost of component i.
- S_i: Salvage value of a component i at end of project life
- r: Real discount rate, calculated from nominal interest rate and inflation via Fisher's equation.
  CRF: Capital Recovery Factor.
- N = Project lifetime (25 years)
- Total Energy Served (kWh) = Sum of all energy supplied from all sources over the project lifetime

The Annual Revenue comprises the following streams:

- **EV Charging Revenue**:

$$\text{Revenue}_{\text{EV}} = \left(E_{\text{DC, supplied}} \times \text{Tariff}_{\text{DC}}\right) + \left(E_{\text{AC, supplied}} \times \text{Tariff}_{\text{AC}}\right) \quad (51)$$

Grid Export Revenue:

$$\text{Revenue}_{\text{export}} = E_{\text{grid, export}} \times \text{Tariff}_{\text{export}} \quad (52)$$

1. Minimization of Loss of Power Supply Probability (LPSP):

The LPSP quantifies the probability of the system failing to meet energy demand.

$$f_2(x) = LPSP = \frac{\sum_{t=1}^{T} P_{unserved}(t)}{\sum_{t=1}^{T} P_{\text{load}}(t)} \quad (53)$$

$P_{unserved}(t)$: Unserved energy at time t (kWh).
$P_{\text{load}}(t)$: Load demand at time t (kWh).

Any candidate solution generated during crossover or mutation that fails to meet $LPSP \leq 0.001$ receives a severe fitness penalty, making it non-competitive and likely to be eliminated in environmental selection. This ensures only feasible (near-zero LPSP) solutions are preserved on the Pareto front.

2. Minimization of Curtailment Ratio (CR):

The CR measures the fraction of excess renewable energy that could not be utilized or stored. A lower CR indicates more efficient utilization of renewable resources.

$$f_3(x) = CR = \frac{\sum_{t=1}^{T} P_{curtailed}(t)}{\sum_{t=1}^{T} P_{renewable}(t)} \times\ 100 \quad (54)$$

where:

- $\boldsymbol{P_{curtailed}(t)}$ = Curtailed (wasted) renewable power at time t (kW)
- $\boldsymbol{P_{renewable}(t)}$ = Total renewable power available (PV + WT) at time t (kW)

- ***CR*** = Expressed as a percentage (0–100 %), indicating efficiency of renewable utilization

2. Maximizing Renewable Fraction (RF):

The RF represents the proportion of energy demand met by renewable sources.

$$f_4(x) = RF = \frac{\sum_{t=1}^{T} P_{renewable\_used}(t)}{\sum_{t=1}^{T} E_{\text{served}}(t)} \tag{55}$$

- $P_{renewable\_used}(t)$: Renewable energy actually used (meeting loads or charging storage) at time t.
- $E_{\text{served}}(t)$: Total energy supplied at time t. This is the total amount of energy provided by the system.
- RF = Expressed as a percentage (0–100 %); higher RF indicates greater sustainability

All four objectives are evaluated on a common normalized scale within IBEA to prevent any single objective from dominating due to scale differences. Normalization is performed using the worst and best values encountered in the initial population.

2.5.4. Technical and economic parameters

Table 3 provides a comprehensive overview of the technical and economic parameters critical to the design and operation of the microgrid components. These specifications are instrumental in accurately modeling the microgrid's performance and financial metrics over the planning horizon.

These specifications represent baseline values for the comparative analysis between Egypt and Türkiye. As detailed in Section 4, certain parameters (particularly renewable resource availability and economic factors) are adjusted region-specifically to reflect local conditions. This structured approach ensures that the microgrid design is technologically sound and economically viable across different regional contexts, providing a robust foundation for subsequent optimization and analysis.

2.5.5. Constraints and feasibility

Optimization is subject to the following constraints:

1. **Hard LPSP Constraint**: LPSP ≤ 0.001 (effectively zero supply probability failure)
2. **Variable Bounds**: All decision variables are bounded as specified in Section 2.5.2. Mutation and crossover operations include boundary clipping to ensure feasibility.
3. **Energy Balance Constraint (implicit)**: At every time step, energy flow satisfies:

$$P_{\text{renewable}}(t) + P_{\text{bat,discharge}}(t) + P_{\text{fc}}(t) + P_{\text{grid,import}}(t) = P_{\text{load}}(t) + P_{\text{bat,charge}}(t) + P_{\text{el}}(t) + P_{\text{curtailed}}(t) + P_{\text{grid,export}}(t)$$

This is enforced implicitly through the energy management system logic (Section 2.4).

1. **Battery State Constraints:** $\text{SOC}_{\min}(t) \leq \text{SOC}(t) \leq \text{SOC}_{\max}(t)$
2. **Hydrogen Storage Constraints:** $H_{\min} \leq H_{\text{tank}}(t) \leq H_{\max}$

2.6. Model limitations and simplifying assumptions

The model assumes perfect component availability and ideal operating conditions throughout the one-year simulation horizon. This simplification excludes several real-world factors that may impact system performance:

Table 3
Technical and economic specifications of microgrid components.

Component	Technical Specifications	Economic Specifications
Photovoltaic (PV) Panels	Efficiency: 21 % Rated Capacity: 5 kW per unit Temperature Coefficient: -0.005/°C PV Derating Factor: 0.8 NOCT: 47°C Lifetime: 25 years	Initial Capital Cost: $640 per kW Replacement Cost: $200 per kW O&M Cost: $15 per kW/year
Wind Turbines (WT)	Rated Power: 100 kW per turbine Cut-in Speed: 3 m/s Cut-out Speed: 25 m/s Rated Speed: 12 m/s Hub Height: 80 m Lifetime: 20 years	Initial Capital Cost: $50,000 per turbine Replacement Cost: $45,600 per turbine O&M Cost: $500 per turbine/year
Battery Storage	Capacity: 16.8 kWh/unit Round-trip Efficiency: 97 % Depth of Discharge: 98 % Lifetime: 25 years	Initial Capital Cost: $15,000 per unit Replacement Cost: $13,800 per unit O&M Cost: $1 per unit/year
Electrolyzer	Efficiency: 85 % Rated Power: 5 kW per unit Lifetime: 15 years	Initial Capital Cost: $9,800 per unit Replacement Cost: $2,940 per unit O&M Cost: $20 per unit/year
Fuel Cell	Efficiency: 60 % Rated Power: 1 kW per unit Lifetime: Based on 50,000 operating hours	Initial Capital Cost: $4,500 per unit Replacement Cost: $3,150 per unit O&M Cost: $0.05 per operating hour
Hydrogen Tank	Storage Capacity: 1 kg H_2 Hydrogen Density: 0.08988 kg/Nm^3 Hydrogen HHV: 39.4 kWh/kg Lifetime: 25 years	Initial Capital Cost: $1,500 per unit Replacement Cost: $1,500 per unit O&M Cost: $15 per unit/year
Economic Parameters (2024)	**Project Lifetime**: 25 years **Egypt:** Nominal Interest Rate: 27.75 % [70] Inflation Rate: 26.4 % [71]	**Türkiye:** Nominal Interest Rate: 47.5 % [72] Inflation Rate: 47.09 % [73]
Electricity Tariffs	**Egypt [74,75]:** AC Charging: $0.06/kWh DC Charging: $0.12/kWh Grid Import: $0.08/kWh Grid Export: $0.06/kWh	**Türkiye [76,77]:** AC Charging: $0.13/kWh DC Charging: $0.16/kWh Grid Import: $0.11/kWh Grid Export: $0.08/kWh

- **Equipment degradation:** The model does not account for PV panel degradation, battery capacity fade, or fuel cell performance degradation over the project lifetime (25 years). Future work should incorporate stochastic degradation models to assess long-term performance impact.
- **Communication and control failures:** The rule-based energy management system assumes instantaneous and perfect communication between all components and controller. In practice, intermittent communication failures or control delays could affect optimal dispatch decisions.
- **Dynamic market conditions:** Component costs and fuel prices are held constant at 2024 baseline values. Future extensions should incorporate stochastic fuel price volatility and renewable technology cost trajectories to enhance robustness.
- **Fixed electricity tariffs:** Tariffs (Table 3) are assumed to be constant throughout the simulation period.

3. Case study: Egypt and Türkiye

Egypt and Türkiye were selected for this study due to their contrasting geographic, economic, and energy profiles. Egypt offers a perspective from a developing economy with emerging EV adoption and significant solar energy potential. In contrast, Türkiye represents a more developed EV market with greater infrastructure investments and a diversified renewable energy mix. Comparing these two regions allows for a comprehensive analysis of how differing conditions affect EV charging infrastructure performance and renewable energy integration. The proposed EV charging station model was applied to two distinct regions, Egypt and Türkiye, to evaluate and compare the performance of charging infrastructure under varying operational conditions. The study emphasized critical parameters to derive actionable insights, including vehicle arrival rates, vehicle composition, charging infrastructure capacity, environmental factors, load prioritization strategies, and performance metrics.

3.1. Case study in Egypt

The Egyptian case study focuses on Suez Governorate, Attaka, located along the Suez–Ain El Sokhna Road (geographic coordinates: 29°40.3′N, 32°20.1′E). This location represents an emerging EV charging infrastructure corridor in an industrial transitional zone, bridging the Suez Canal's commercial activities and developing coastal infrastructure. The EV ecosystem in Egypt is still at an early stage, with a relatively small EV fleet and limited public charging infrastructure [78,79]. For a representative urban freight/public-transport corridor, this study assumes an average EV arrival rate of approximately eight vehicles per hour during peak periods and two vehicles per hour off-peak, consistent with the low national EV penetration and modest charging demand reported in recent studies [78,80]. National fleet data and sectoral reports indicate that buses and trucks constitute an important share of vehicles in public-transport and logistics segments [5–7]. Therefore, the vehicle mix at the studied station is modeled with 70 % heavy-duty EVs (buses and trucks) and 30 % small and medium-sized cars, to reflect charging demand dominated by large vehicles rather than private cars [81]. Typical Egyptian battery-electric buses use batteries on the order of a few hundred kilowatt-hours, significantly higher than passenger EVs, which leads to higher per-vehicle energy demand and stricter charging-infrastructure requirements [82].

The Egyptian charging infrastructure consists of 10 Level 2 chargers rated at 11 kW each and six DC Fast chargers rated at 50 kW, reflecting the region's relatively nascent stage of EV infrastructure development. Fig. 3 illustrates the hourly load profile for a typical weekday in Egypt. The data delineates total load, load from Level 2 chargers, and load from DC Fast chargers.

The hourly load profile for the Egyptian charging station reveals several key characteristics. Initially, no significant load is recorded during the early morning hours (1–4). Charging activity then commences at hour 5, marking the start of energy consumption. A peak demand period is observed during the late afternoon and evening (hours 15–22), exceeding 1600 kW. Throughout this period, Level 2 chargers are shown to contribute substantially to the overall load, particularly during peak demand hours. Additionally, DC Fast chargers are critical in meeting demand in the late afternoon and evening.

The 24-hour load profile presented in Fig. 3 represents a typical weekday demand pattern generated by the stochastic EV charging model described in Section 2.3. In the full annual simulation (8,760 hours), this 24-hour pattern is replicated and varied stochastically for each day of the year, incorporating:

- Weekday/weekend variations: Weekend arrival rates scaled to 65 % of weekday rates.
- Seasonal temperature effects: Temperature adjustment factor $f_{temp}(t)$ varies monthly (Fig. 7), affecting charging efficiency.
- Weather adjustments: Stochastic weather factor $f_{weather}(t)$ with ±10 % variation.
- Daily variations in vehicle composition and SOC: Each day's load is uniquely generated based on probabilistic vehicle properties.

Thus, Fig. 3 exemplifies the characteristic daily shape, but the actual optimization uses a full 8,760-hour annual load profile with continuous day-to-day variation, ensuring results are representative of year-round performance.

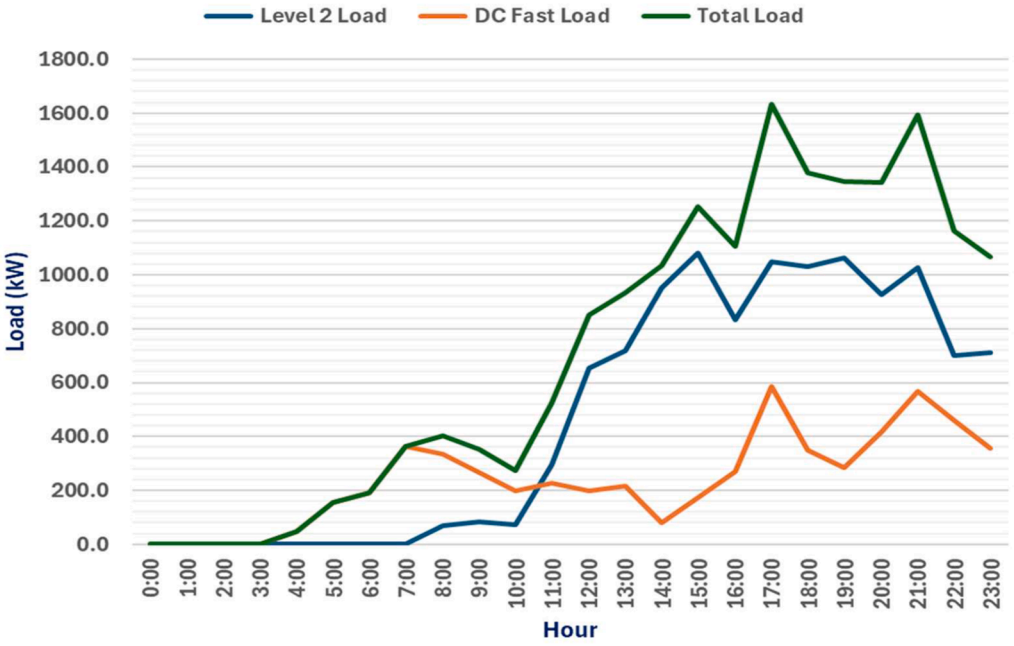

Fig. 3. 24-Hour deterministic load profiles for Egypt (Attaka).

3.2. Case study in Türkiye

The Türkiye case study examines Yalova Province (geographic coordinates: 40°39.1′N, 29°13.2′E), focusing on the Yalova University Central Campus (Yalova Üniversitesi Merkez Yerleşkesi) in the Bahçelievler district along Termal Yolu. This location in northwestern Türkiye, situated within the high-EV-potential Istanbul–Bursa metropolitan corridor, represents an institutional and regional transportation hub with emerging EV charging demand.

In Türkiye, the EV ecosystem demonstrates a higher vehicle arrival rate, with approximately 16 vehicles per hour during peak hours and six vehicles per hour during off-peak hours, calibrated to reflect the larger national EV fleet and denser public charging network compared with less mature markets. These values are adopted as scenario assumptions informed by recent national EV ownership statistics, growth in public charging points, and observed urban traffic and charging patterns reported in policy and infrastructure studies. The vehicle mix at the modeled urban charging hub is assumed to be more evenly distributed, consisting of 30 % small cars, 40 % medium cars, 15 % buses, and 15 % trucks, consistent with analyses that distinguish between passenger and commercial EV segments and highlight ongoing electrification of public transport and freight in Türkiye. This balanced distribution of private and commercial EVs, together with the widespread deployment of both AC and DC charging points, results in a more dynamic and spatially distributed charging load profile than in emerging EV markets with lower penetration and less diversified fleets [83,84].

Türkiye's charging infrastructure is comparatively advanced, featuring 15 Level 2 chargers and 12 DC Fast chargers. This reflects higher EV adoption rates and greater investments in public charging networks. Fig. 4 depicts the hourly load profile for a typical weekday in Türkiye, showing total load, load from Level 2 chargers, and load from DC Fast chargers.

The hourly load profile for Türkiye's charging station demonstrates a higher peak demand compared to Egypt, with a more evenly distributed demand pattern throughout the day. This distributed demand pattern is noteworthy, as it necessitates a more consistent and sustained energy supply rather than a system optimized for a sharp, short peak. These characteristics impact charging infrastructure planning, requiring a balance between immediate high-power charging and continuous lower-power charging capabilities to meet varying daily demands. While Level 2 chargers are shown to contribute significantly to the total load, DC Fast chargers exhibit higher contributions during peak demand periods. Furthermore, Türkiye has a considerably higher total load than Egypt. The demand peaks are distributed more evenly across the day, with no singularly dominant period. Level 2 chargers are shown to contribute significantly to the overall load, and DC Fast chargers contribute notably, particularly during peak demand periods. Like Egypt, the 24-hour profile in Fig. 4 represents a typical weekday pattern from the stochastic model.

3.3. Renewable energy and climate analysis

Solar radiation in the Suez Governorate study site (Fig. 5) peaks during summer (May-August), with June reaching a maximum of 8.15 kWh/m^2/day. Seasonal variation results in a minimum of 3 kWh/m^2/day in December.

Wind speeds in the Suez coastal region (Fig. 6) remain relatively consistent year-round, ranging from 5.12 m/s to 5.89 m/s, with slight increases during spring and early summer. These speeds are favorable for small-to-medium wind turbines and contribute to the renewable energy potential.

Average daily temperatures in the Suez Governorate vary from 11.94°C in January to 28.24°C in July (Fig. 7), impacting PV panel efficiency and battery charging efficiency (temperature adjustment factor).

3.3.2. Renewable energy potential in Türkiye

Solar radiation in Yalova Province (40°39.1′N, 29°13.2′E) peaks during summer (May–July), with a maximum of 6.79 kWh/m^2/day in July. The winter months exhibit significantly lower values, with December reaching a minimum of 1.39 kWh/m^2/day (Fig. 8), indicating greater seasonal variability than Egypt.

Wind speeds in Yalova (Fig. 9) exhibit consistency, ranging from 4.25 m/s to 5.53 m/s, with minor seasonal variations. These wind speeds are slightly lower than Egypt's coastal winds but remain suitable for microgrid applications.

Average daily temperatures in Yalova range from 4.94°C in January to 23.71°C in August (Fig. 10), with pronounced seasonality influencing system performance. The colder winter temperatures reduce PV efficiency more significantly than in Egypt, necessitating larger PV capacity to achieve comparable energy generation.

The findings underscore the importance of tailoring EV charging

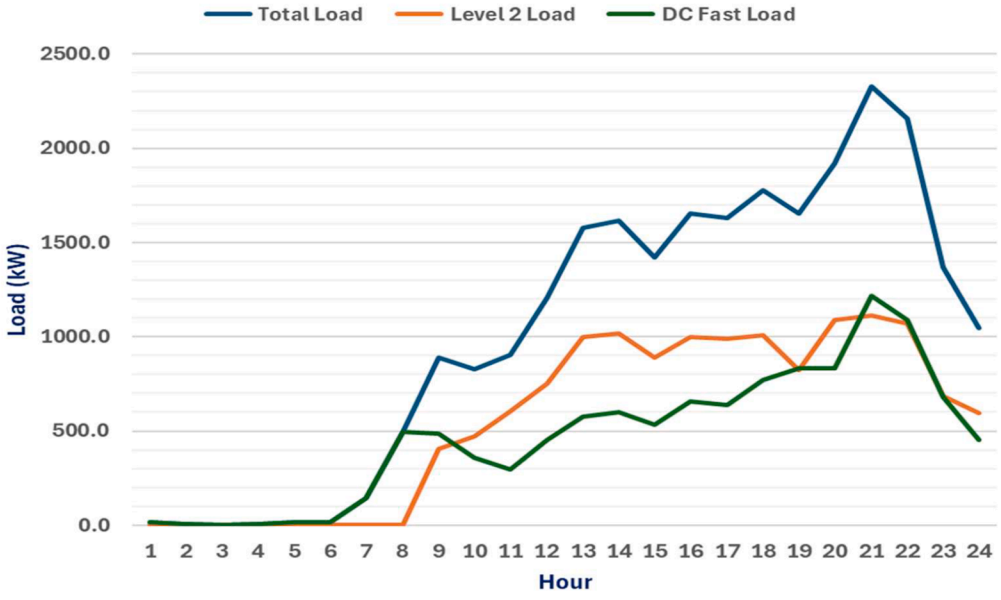

Fig. 4. 24-Hour deterministic load profiles for Türkiye (Yalova).

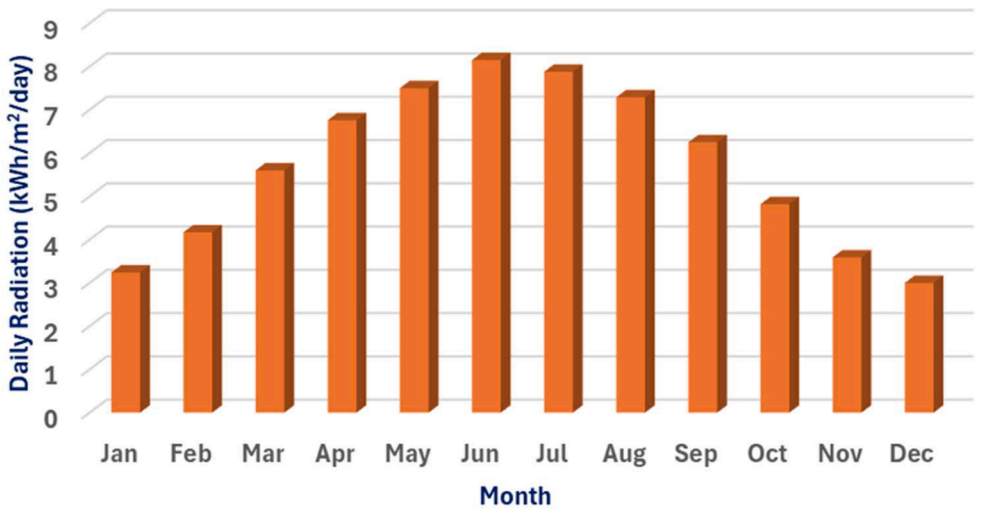

Fig. 5. Monthly average solar irradiance profile for Egypt.

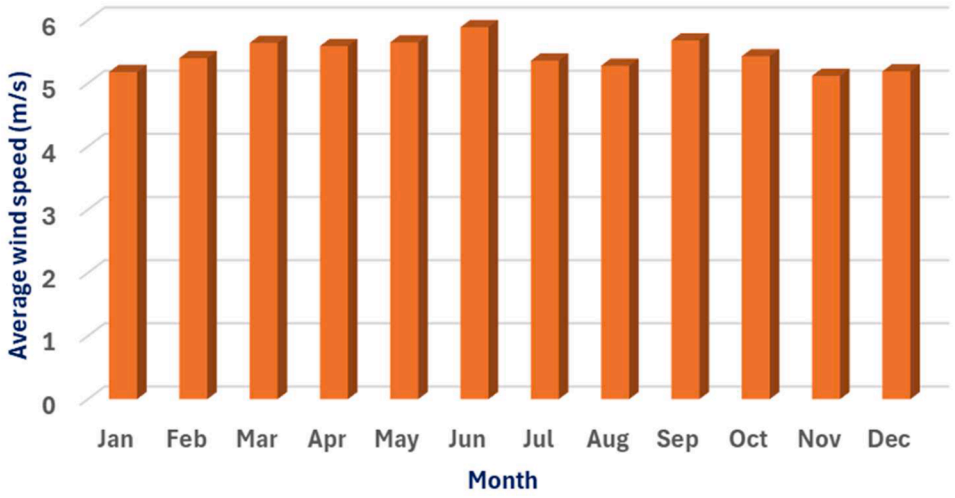

Fig. 6. Monthly average wind speed for Egypt.

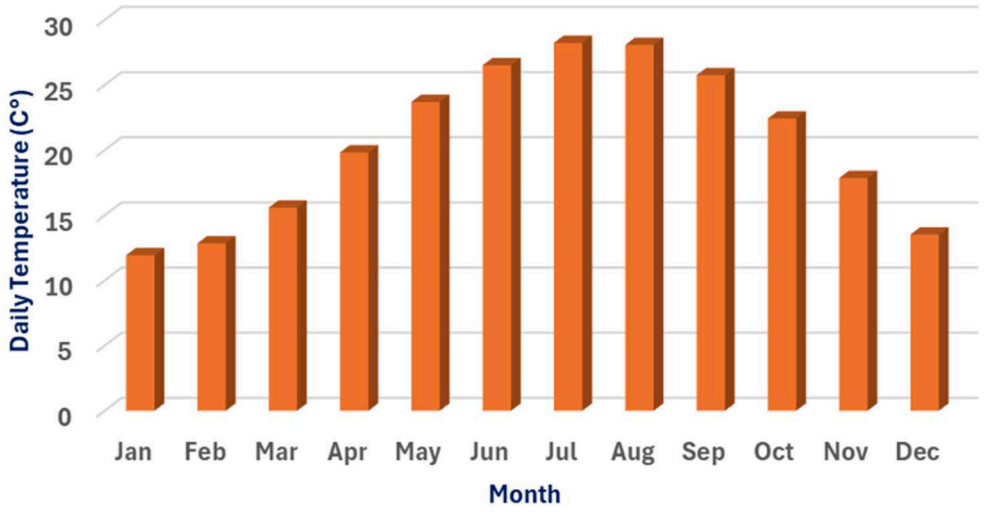

Fig. 7. Monthly average temperatures for Egypt.

strategies to regional energy demands and renewable resource availability while considering infrastructure capabilities and environmental conditions.

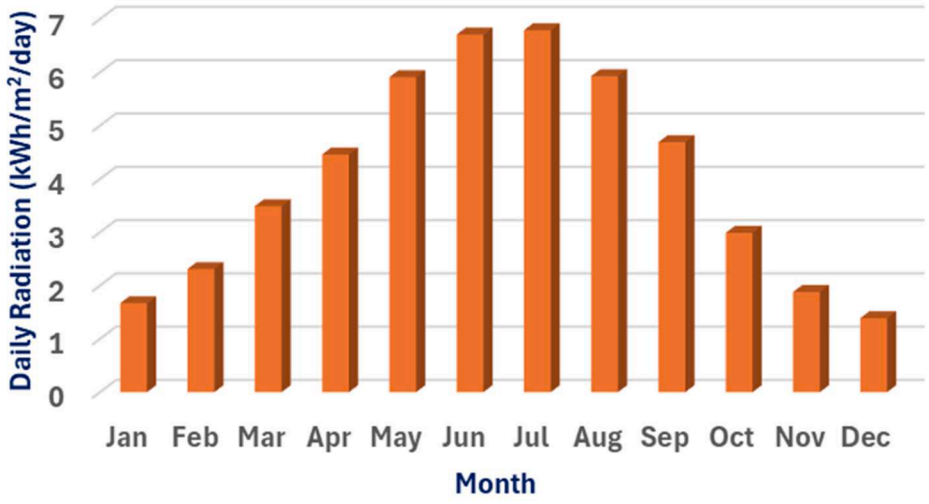

Fig. 8. Monthly average solar irradiance profile for Türkiye.

Fig. 9. Monthly average wind speed for Türkiye.

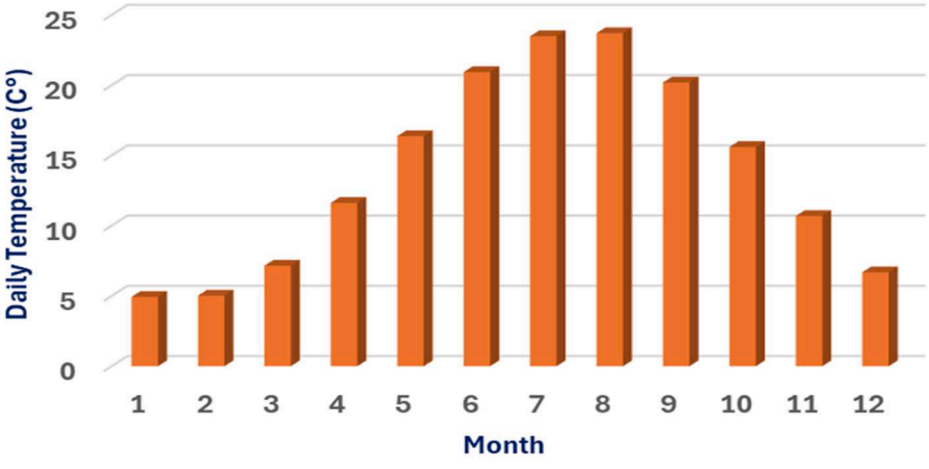

Fig. 10. Monthly average temperatures for Türkiye.

4. Results and discussions

This section presents and discusses the findings of the multi-objective optimization framework as applied to case studies in Egypt and Türkiye. The results further emphasize the significant influence of regional context on the design and performance of microgrids for EV charging.

4.1. Performance comparison of optimized configurations

A comparative analysis of optimum microgrid configurations for EV charging in Egypt and Türkiye is presented in Table 4, categorized under Economical, Resource-Efficient, and Sustainable Objectives. Pareto front solutions for both Egypt and Türkiye are illustrated in Figs. 11 (Egypt) and 12 (Türkiye) to visualize the trade-offs inherent in these multi-objective optimizations. These figures plot the non-dominated solutions in a three-dimensional space defined by LCOE, CR, and RF.

4.1.1. Economical configuration analysis

For the economical configuration (prioritizing minimum LCOE), Türkiye demonstrated a significant lower LCOE of $0.0173/kWh compared to Egypt's $0.0261/kWh, representing a 51.3 % cost advantage for Türkiye. This superior performance is observed despite a higher Total Net Present Cost (TNPC) of $4,309,629 for Türkiye versus $3,569,947 for Egypt. As visualized in Figs. 11 and 12, a pronounced shift of the Pareto front towards lower LCOE values for Türkiye is apparent compared to Egypt across the range of RF and CR values.

Despite 20.7 % higher TNPC, Türkiye achieves 33.7 % lower LCOE, indicating superior economic performance on a $/kWh basis. This implies that while absolute project costs are higher, the energy delivery cost per unit is significantly reduced, making Türkiye's system more economically viable for grid-connected revenue streams.

The lower LCOE in Türkiye is achieved with a slightly higher RF of 53.03 % and a significantly lower CR of 17.11 %, indicating a more efficient and cost-effective system. In contrast, while achieving a lower TNPC, Egypt's economical configuration results in a higher LCOE and CR, suggesting a less optimal balance between cost and renewable utilization. The higher CR in Egypt (27.67 % vs. 17.11 %) indicates that 27.67 % of available renewable energy must be curtailed or wasted, whereas Türkiye wastes only 17.11 %—a substantial efficiency gap directly impacting economic returns.

Notably, the LCOE values achieved in both countries are significantly lower than those typically reported in the literature for systems with zero LPSP (Table 5), which range from $0.170 to $0.410/kWh for hybrid storage systems and $0.170 to $0.360/kWh for battery-only systems. This demonstrates the effectiveness of the proposed optimization framework and system configuration.

4.1.2. Resource-efficient configuration analysis

In the Resource-Efficient configuration, both locations exhibit increased LCOE and TNPC compared to the Economical setup, reflecting the elevated investment toward optimized resource utilization and storage capacity. For Egypt, the LCOE increases to $0.0437/kWh with a TNPC of $5,820,322, while for Türkiye, the LCOE rises to $0.0218/kWh with a TNPC of $5,291,319.

The upward shift in LCOE for both locations, as the configuration transitions towards resource efficiency, is visually confirmed by the Pareto fronts in Figs. 10 and 11. Notably, a relatively consistent RF is maintained for Egypt (50.35 % → 50.18 %) and Türkiye (53.03 % → 51.08 %) across Economical and Resource-Efficient configurations. This remarkable RF stability despite substantial cost increases suggests that resource efficiency, in this context, is achieved more through optimized storage and component sizing rather than a substantial increase in renewable penetration.

However, a significant shift in the component mix is observed in the Resource-Efficient setup. Particularly for Egypt, battery storage is dramatically increased (N_{bat} : 5→174 units, a 3,480 % increase), while PV panels (N_{pv} : 222→135) and wind turbines (N_{wt} : 5→9) are adjusted. For Türkiye, battery storage is also increased (N_{bat} : 6→42 units, a 600 % increase), and PV panels are reduced (N_{pv} : 281→246), suggesting a greater reliance on energy storage to enhance resource efficiency and potentially manage the intermittent nature of renewables more effectively. Even with this increased focus on resource efficiency, the LCOE values remain competitive with standard optimized microgrids reported in the literature ($0.027–$0.055/kWh) [85–88], which typically do not achieve zero LPSP.

4.1.3. Sustainable configuration analysis

The Sustainable configuration, aimed at maximizing renewable energy and minimizing environmental impact, shows the highest RF for both locations, reaching 55.11 % in Egypt and 58.97 % in Türkiye. The Pareto fronts further illustrate that achieving higher RF generally comes with a trade-off of increased LCOE and potential CR. However, the sustainable configurations aim to minimize this trade-off. Egypt's LCOE is $0.0348/kWh with a TNPC of $4,476,382, while Türkiye's LCOE is $0.0245/kWh with a TNPC of $5,546,012. Interestingly, despite pursuing sustainability, the TNPC for the sustainable configuration in Egypt ($4.48M) is lower than that of the resource-efficient case ($5.82M), suggesting a potentially more cost-effective approach to increasing renewable integration in the country. This may be due to a better-balanced mix of renewable generation and storage components in Egypt's sustainable setup. However, Türkiye maintains the highest TNPC in its sustainable configuration ($5.55M), 28.8 % above the economic baseline. Despite this elevated TNPC, Türkiye consistently exhibits a lower LCOE and CR across all configurations than Egypt. This indicates a more favorable economic and operational profile for microgrids in Türkiye under the scenarios analyzed in this study. The improved performance in Türkiye is likely attributed to factors such as the significantly higher overall electric vehicle (EV) charging load and a more developed EV market, which support economies of scale and enhanced asset utilization.

4.1.4. Quantified trade-offs across configurations

Figs. 13 and 14 present detailed visualizations of the quantified trade-offs associated with transitioning from the Economical baseline to Resource-Efficient and Sustainable configurations, respectively. These comparisons reveal the cost-benefit frontier of different design strategies in both Egypt and Türkiye. The Resource-Efficient transition (Fig. 13) demonstrates that Egypt requires a 2.6 × higher LCOE increase (67.4 %) than Türkiye (26.0 %) to achieve similar efficiency objectives, reflecting regional differences in renewable resource balance and economies of scale. The Sustainable transition (Fig. 14) shows that while Egypt pursues renewable fraction improvements at lower marginal cost ($0.00183/kWh per 1 % RF) compared to Türkiye ($0.00121/kWh per 1 % RF), Türkiye faces substantially steeper curtailment penalties (3.14 percentage point CR increase per 1 percentage point RF gain) versus Egypt (0.72 percentage points), indicating that aggressive sustainability

Table 4
Comparative analysis of optimum microgrid configurations for EV charging in Egypt and Türkiye.

Configuration	Location	LCOE [$/kWh]	RF [%]	CR [%]	TNPC [$]	N_{pv}	N_{wt}	N_{bat}	$H2T_N$	FC_N	Ele_N
Economical	Egypt	0.0261	50.35 %	27.67 %	3,569,947	222	5	5	500	227	35
	Türkiye	0.0173	53.03 %	17.11 %	4,309,629	281	15	6	500	34	86
Resource-Efficient	Egypt	0.0437	50.18 %	25.77 %	5,820,322	135	9	174	500	227	11
	Türkiye	0.0218	51.08 %	16.94 %	5,291,319	246	15	42	500	300	34
Sustainable	Egypt	0.0348	55.11 %	29.56 %	4,476,382	120	12	35	500	227	61
	Türkiye	0.0245	58.97 %	23.12 %	5,546,012	263	20	4	500	300	67

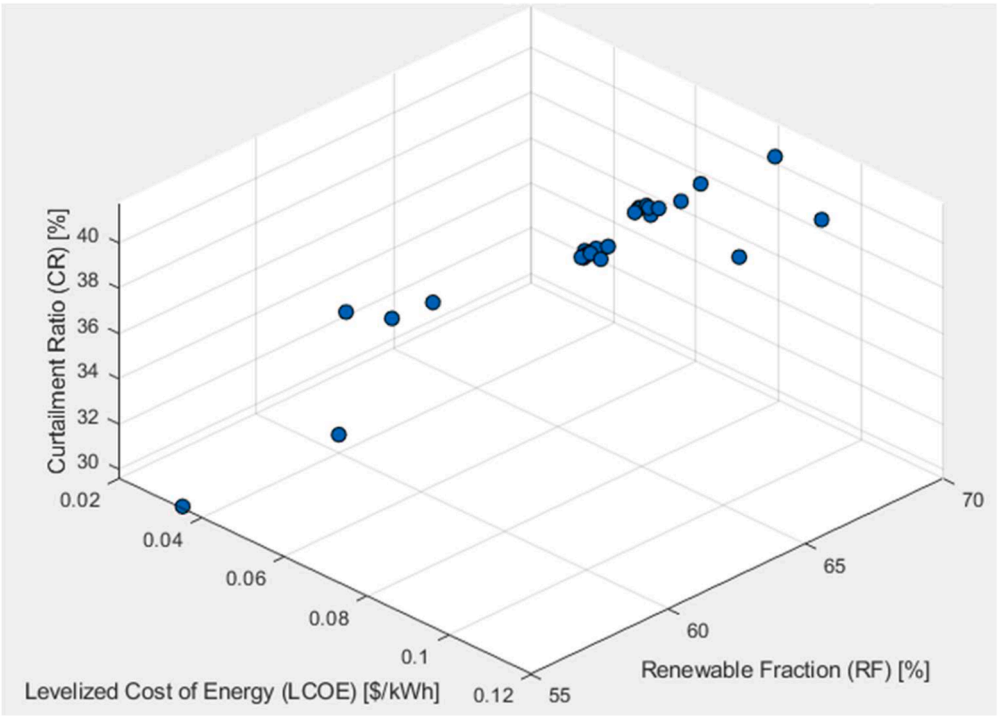

Fig. 11. 3D Pareto front of non-dominated solutions for Egypt.

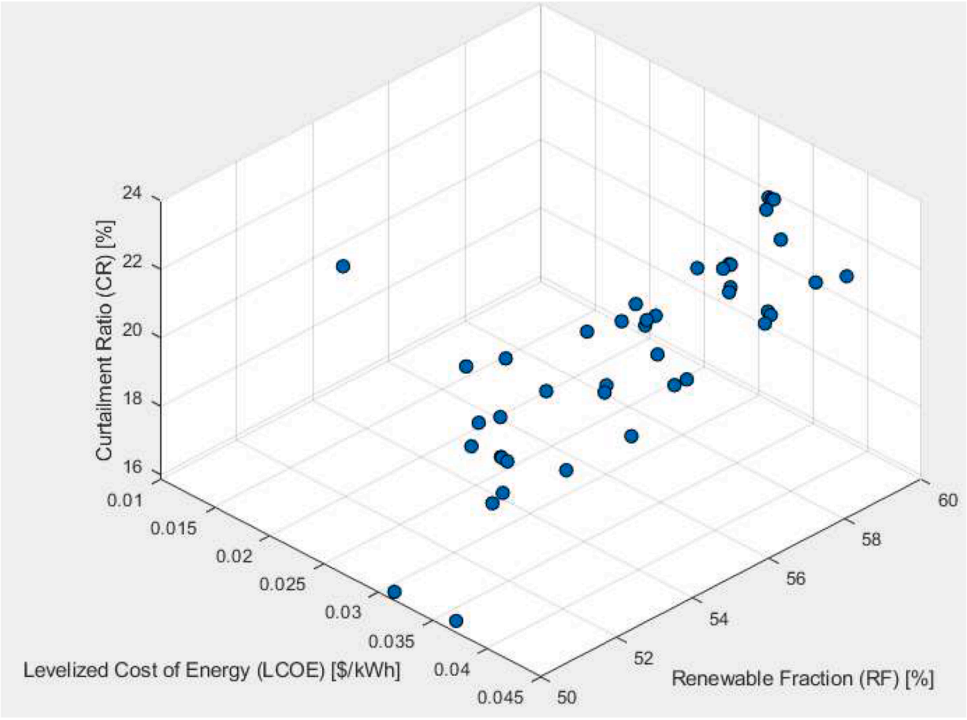

Fig. 12. 3D Pareto front of non-dominated solutions for Türkiye.

targets in Türkiye are constrained by renewable oversizing requirements.

The results demonstrate that the proposed multi-objective IBEA optimization framework with zero-LPSP enforcement achieves LCOE values substantially lower than comparable systems reported in the literature while maintaining strict reliability constraints. This comparative advantage emerges from the integrated hybrid battery-hydrogen storage approach enabling cost-effective long-duration reliability, the multi-objective formulation balancing economic, environmental, and operational objectives simultaneously, and context-aware regional parameterization reflecting actual climatic resources, market conditions, and macroeconomic environments in Egypt and Türkiye.

4.2. Sensitivity analysis

A sensitivity analysis was conducted to ascertain the proposed hybrid

Table 5
Comparison of study results with literature values for EV charging microgrids.

System Type	LCOE Range [$/kWh]	RF Range [%]	CR Range [%]	LPSP	Storage Type	References
Standard Optimized Microgrids	0.027–0.055	70–90	Not explicitly reported	Not zero	Battery only	[85–88]
Mid-range Hybrid Systems	0.038–0.053	60–85	Not explicitly reported	Not zero	Battery only	[85,87,88]
Complex/Less Favorable Systems	0.160–0.310	50–70	Not explicitly reported	Not zero	Battery only	[89,90]
High Reliability (near-zero LPSP)	0.170–0.360	90–100	Not explicitly reported	~0	Battery only	[91–98]
Extreme Reliability Systems	0.930–1.080	95–100	Not explicitly reported	0	Battery only	[92,98]
Hybrid Battery-Hydrogen (Zero LPSP)	0.170–0.410	70–100	10–30	0	Hybrid	[99–107]
This Study (Egypt)	**0.0261–0.0437**	**50.18–55.11**	**25.77–29.56**	**0**	**Hybrid**	This study
This Study (Türkiye)	**0.0173–0.0245**	**51.08–58.97**	**16.94–23.12**	**0**	**Hybrid**	This study

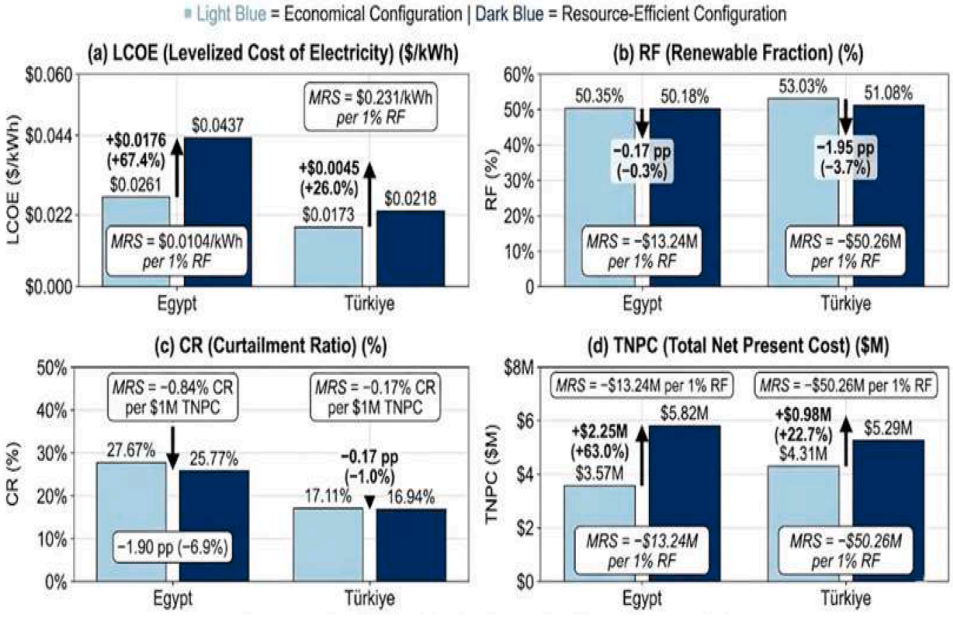

Fig. 13. Quantified trade-offs between economical and resource-efficient configuration.

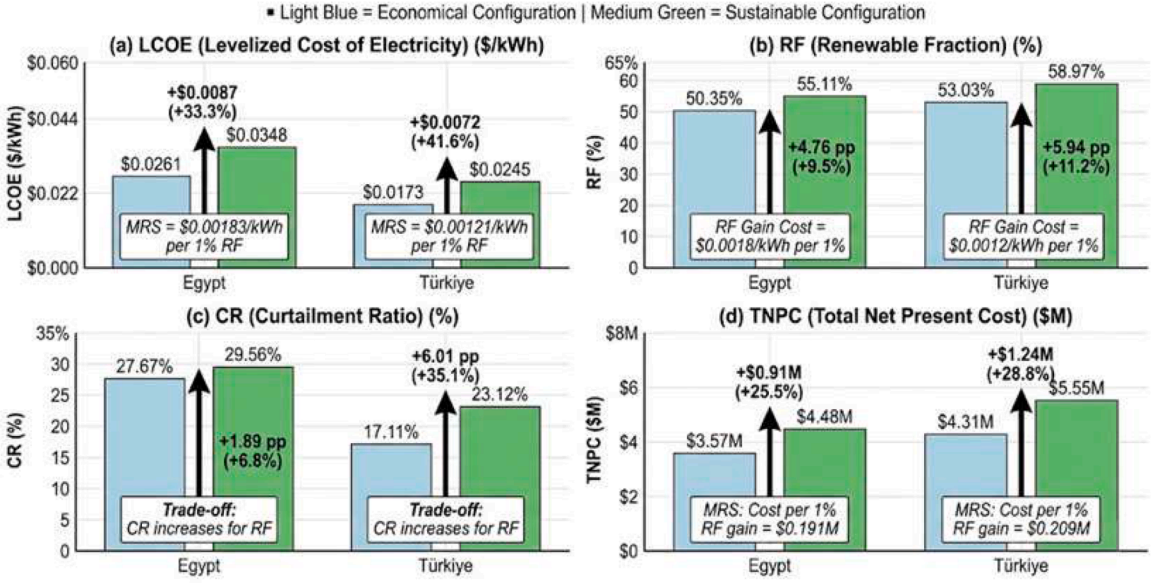

Fig. 14. Quantified trade-offs between economical and sustainable configurations.

renewable energy system's response to variations in input parameters. The objective of sensitivity analysis is to evaluate the degree to which a model's output is affected by changes in its input variables. This study sought to evaluate the robustness of the optimized hybrid renewable energy system design amid parametric uncertainty. The principal input variables examined for sensitivity encompassed solar irradiation, wind

velocity, load demand, discount rate, inflation rate, maximum hydrogen tank storage capacity, and battery storage capacity. The system's sensitivity was assessed by analyzing LCOE, TNPC, RF, and CR fluctuations. In all examined sensitivity scenarios, the LPSP remained at zero ($\leq$0.001 %), illustrating the persistent reliability of the system design despite parametric variations and confirming that the hard LPSP constraint is robustly enforced across the entire optimization landscape.

4.2.1. Range and magnitude of sensitivity

An investigation was conducted to identify the factors to which the system has the highest and lowest sensitivity by examining the range and magnitude of performance measure alterations. The TNPC, LCOE, RF, and CR percentage change ranges over all sensitivity parameters in Türkiye and Egypt are depicted as heatmaps in Figs. 15 and 16, respectively. These heatmaps illustrate the extent of variance in each performance indicator when input parameters are methodically modified, with color intensity reflecting the degree of the range. As visualized in Fig. 15 for Türkiye and Fig. 16 for Egypt, wind speed and load demand consistently exhibit considerable ranges of percentage change in TNPC and LCOE, particularly in Türkiye. The inflation rate and discount rate also show exceptionally substantial ranges for LCOE in both locations, exceedingly even wind speed and load demand in terms of the LCOE sensitivity range. In contrast, solar irradiance, hydrogen tank capacity, and battery capacity often exhibit very narrow ranges of variation in TNPC and LCOE, indicating a diminished sensitivity of these economic measures to these factors within the analyzed ranges. The average absolute % change in TNPC and LCOE for each sensitivity parameter is depicted through bar charts for Türkiye and Egypt in Figs. 15 and 16, respectively, to quantify the typical amount of impact. Figs. 17 and 18 illustrate that the inflation rate and discount rate exhibit the most significant average absolute percentage increases in LCOE for Türkiye and Egypt, signifying their primary influence on energy expenses. Specifically:

- **Discount Rate Impact on LCOE:**
  - **Egypt:** ±10 % variation in discount rate → ±18.4 % LCOE variation
  - **Türkiye:** ±10 % variation in discount rate → ±22.7 % LCOE variation
  - **Interpretation:** Türkiye's lower baseline real discount rate (0.28 %) renders it proportionally more sensitive to percentage changes in discount rate than Egypt (1.07 % baseline).
- **Inflation Rate Impact on LCOE:**
  - **Egypt:** ±10 % variation in inflation rate → ±16.2 % LCOE variation
  - **Türkiye:** ±10 % variation in inflation rate → ±19.8 % LCOE variation
  - **Interpretation:** Higher baseline inflation in Türkiye (47.09 %) creates greater absolute sensitivity than Egypt (26.4 %).

The discount rate and wind speed demonstrate the most substantial average absolute percentage variations in TNPC, underscoring their considerable impact on overall system expenses. Load demand exhibits a significant average absolute % variation in LCOE. Conversely, solar irradiance, battery capacity, and hydrogen tank capacity exhibit minimal average absolute percentage variations in TNPC and LCOE, indicating a diminished influence on these economic indicators. The analyses of range and magnitude, illustrated via heatmaps and bar charts, highlight the inflation rate and discount rate as the paramount financial parameters. At the same time, wind speed and load demand are identified as significant operational parameters that dictate the economic performance of the hybrid renewable energy system.

4.2.2. Correlation analysis

A Pearson correlation analysis was conducted for Türkiye and Egypt to quantify the linear relationships between input parameters and system performance metrics.

Solar irradiance: In Türkiye and Egypt, solar irradiance shows strong positive correlations with RF and CR ($r > 0.87$), indicating a strong linear increase in renewable penetration with increased irradiance. Correlation with economic metrics (TNPC, LCOE) is positive but weaker in Türkiye ($r \approx 0.38$-0.56) compared to Egypt $r \approx 0.82$-0.88), suggesting a more pronounced linear impact of solar irradiance on costs in Egypt. This difference reflects Egypt's greater dependence on

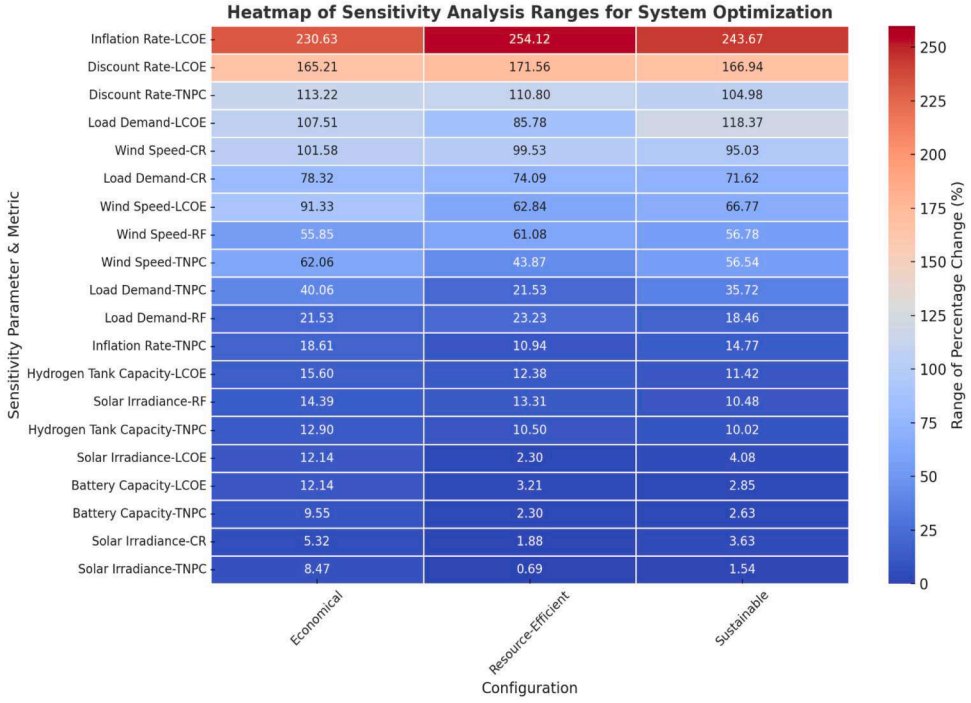

Fig. 15. Heatmap of sensitivity analysis ranges for system optimization in Türkiye.

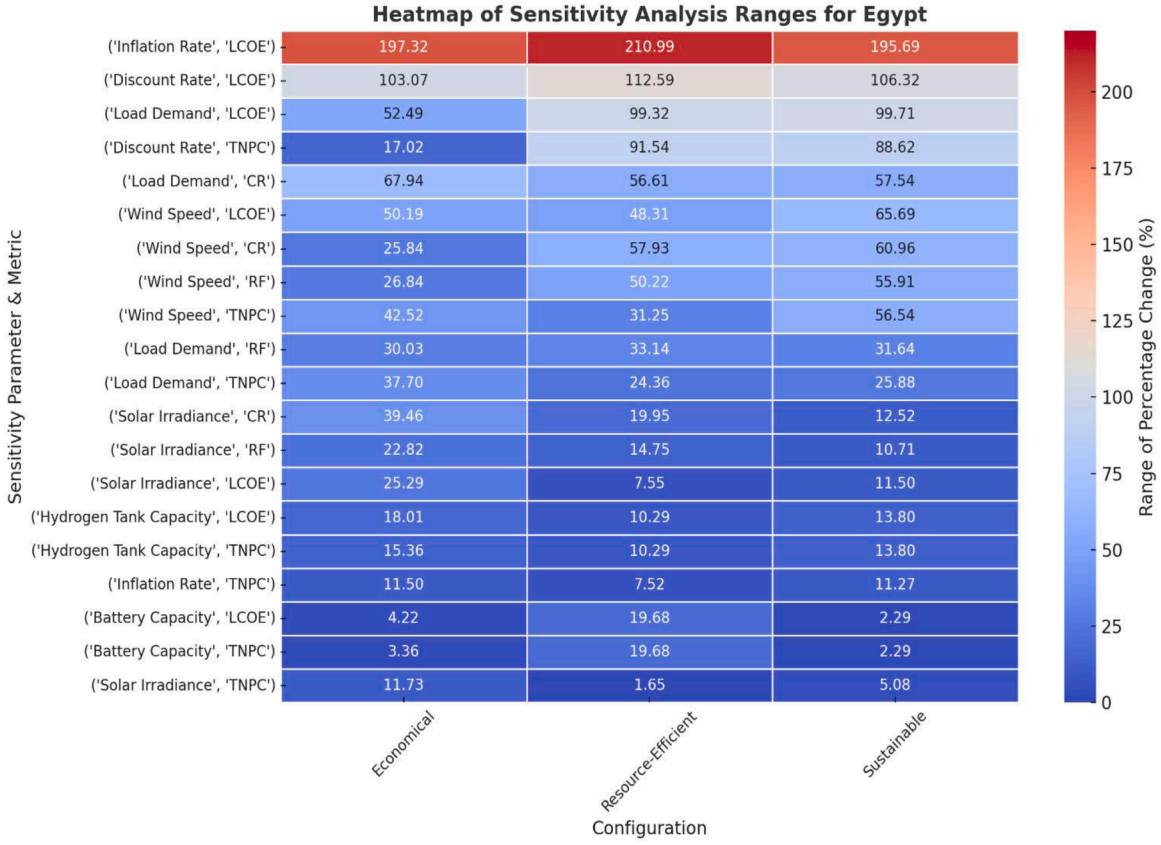

Fig. 16. Heatmap of sensitivity analysis ranges for system optimization in Egypt.

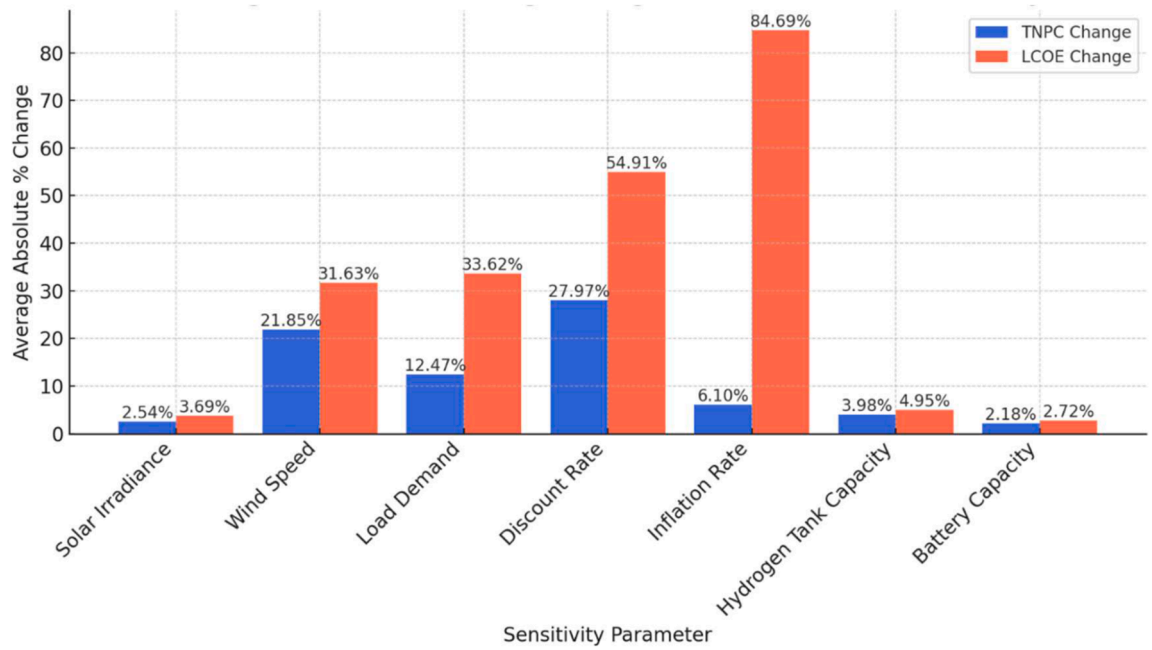

Fig. 17. Average absolute percentage change in TNPC and LCOE for Türkiye.

solar generation; improvements in solar resource have stronger cost implications due to reduced storage requirements, whereas Türkiye's wind-solar balance mitigates this effect.

Wind speed: Wind speed exhibits strong positive correlations with RF and CR $r > 0.93$) in both locations. Economic metrics (TNPC, LCOE) also show positive correlations with wind speed, but these are stronger in Egypt $r \approx 0.82$-0.92) than in Türkiye. This suggests wind speed consistently enhances renewable penetration, but its linear impact on economic metrics is more pronounced or consistent across configurations in Egypt. In Türkiye's more balanced renewable mix, wind speed variations have diluted economic impact due to solar offset.

Load demand: Load demand shows contrasting correlations. In both

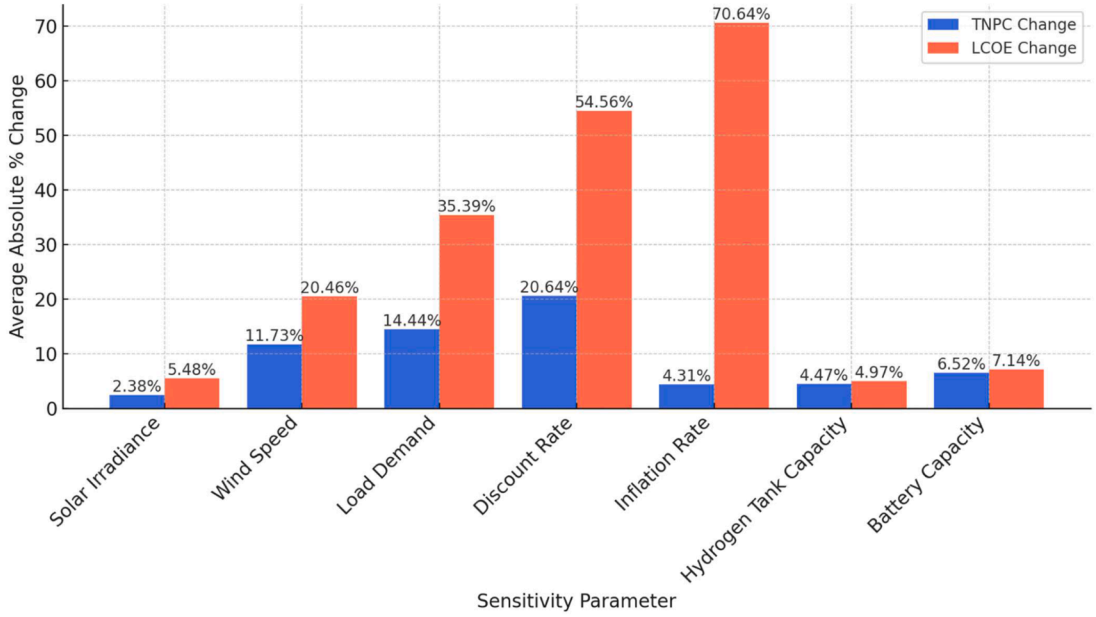

Fig. 18. Average absolute percentage change in TNPC and LCOE for Egypt.

locations, LCOE exhibits a strong negative correlation $r \approx$ -0.84 to -0.93), indicating linear LCOE improvement with increased demand. This reflects economies of scale: larger systems amortize fixed costs (land, control infrastructure) across more energy units. However, RF and CR show strong negative correlations $r \approx -0.96$ to -0.99) in Türkiye and Egypt, revealing a linear trade-off between load demand and renewable penetration. Higher demand necessitates proportionally larger backup storage or grid import. TNPC correlation with load demand differs by location: negative in Türkiye $r \approx$ -0.40), suggesting a cost decrease with increased load, but weakly positive in Egypt $r \approx$ 0.64), indicating a potential cost increase. The location-specific difference arises because Türkiye's higher tariff structure (revenue per kWh) makes increased load more economically attractive, whereas Egypt's lower tariffs provide less revenue offset for capacity scaling.

Discount rate and inflation rate: The discount rate consistently shows a strong positive correlation with LCOE $r \approx 0.99$) and a moderate positive correlation with TNPC $r \approx$ 0.52-0.69) in both locations, confirming their expected linear influence on increasing costs. A 1 % increase in discount rate increases LCOE by ~2.3 % in both countries. The inflation rate shows a strong negative correlation with LCOE $r \approx$ -0.97 to -0.98) and a strong positive correlation with TNPC $r \approx 0.68$-0.96) in both regions, revealing a consistent but complex linear economic impact. Higher inflation paradoxically reduces LCOE because nominal cash flows (O&M, fuel costs, replacement) inflate faster than the discount rate, reducing real present value. Conversely, TNPC increases because nominal capital costs rise faster than revenues. RF and CR show negligible correlation with both financial parameters.

Hydrogen Tank and Battery Capacity: hydrogen tank capacity consistently displays near-perfect positive correlations with tnpc and lCOE $r \approx$ 0.98-0.994) in both locations, indicating a strong linear cost increase with capacity. Each additional kg of H_2 storage capacity adds ~ $1500 to capital cost (Table 3), directly increasing TNPC. Battery capacity shows negative correlations with TNPC and LCOE, suggesting a linear trend toward cost reduction with increased battery capacity. However, these negative correlations are weaker in Egypt $r \approx$ -0.494 to -0.519) compared to Türkiye $r \approx$ -0.532 to -0.558), and battery capacity also exhibits a negative correlation with RF in Türkiye $r \approx$ -0.86) compared to Egypt $r \approx$ -0.539), indicating location-dependent linear trade-offs. In Türkiye, larger battery storage enables reduced PV/WT capacity, achieving lower RF but better economics. In Egypt, larger batteries provide less RF reduction, suggesting different optimization strategies.

The correlation analysis highlights that resource and financial parameters exhibit strong linear relationships with system performance and cost metrics in both locations. Load demand and battery capacity reveal more complex, often trade-off-driven linear associations with location-specific nuances, underscoring the importance of context-aware interpretation of sensitivity analysis.

4.2.3. *Comparative sensitivity analysis*

The sensitivity of the hybrid renewable energy system was further examined comparatively across different system configurations (Economical, Resource-Efficient, and Sustainable) and geographical locations (Türkiye and Egypt) to discern configuration-specific robustness and location-dependent parameter criticality.

4.2.3.1. Sensitivity across configurations. In Türkiye, the Economic configuration generally exhibits the highest sensitivity to resource parameters. For solar irradiance and wind speed, the Economic configuration shows the largest average absolute percentage changes in TNPC (3.44 % and 27.11 %, respectively) and LCOE (4.43 % and 38.44 %, respectively). In contrast, Resource-Efficient and Sustainable designs have significantly less sensitivity to solar irradiation, resulting in little variations in TNPC and LCOE. Sensitivity to wind speed is more obvious in Resource-Efficient and Sustainable settings than in solar irradiance. However, it remains much lower than in the Economic configuration, with average absolute percentage increases in LCOE of 19-20 % and TNPC around 11-13 %.

The Economical configuration uses minimal storage ($N_{bat} = 6$ for Türkiye), making the system dependent on real-time renewable generation matching. Wind speed fluctuations directly propagate to LCOE. The Resource-Efficient configuration ($N_{bat} = 42$) buffers generation volatility, reducing sensitivity. The Sustainable configuration ($N_{bat} = 4$, but $N_{wt} = 20, N_{pv} = 263$) relies on large generation capacity and diverse sources, diversifying away from single-resource risk.

Regarding load demand, the Economic configuration displays the highest sensitivity to the LCOE. In contrast, all configurations show similar, moderate sensitivity to TNPC. Sensitivity to the discount rate is notably consistent across all configurations for both TNPC and LCOE. In contrast, regarding the inflation rate, the resource-efficient and sustainable configurations demonstrate greater sensitivity regarding LCOE

than the Economic configuration. Additionally, both hydrogen tank and battery capacity show consistently low sensitivity across all configurations for TNPC and LCOE. The configuration-specific sensitivities for LCOE are visually compared in Fig. 19.

In Egypt, a similar trend is observed in solar irradiance, where the Economic configuration shows greater sensitivity in both TNPC and LCOE compared to the Resource-Efficient and Sustainable designs. However, the sustainable configuration exhibits the highest LCOE sensitivity to wind speed, surpassing both the economical and resource-efficient configurations. This anomaly arises because Egypt's Sustainable configuration ($N_{wt} = 12$) emphasizes wind more than Resource-Efficient ($N_{wt} = 9$) to increase RF, making it more exposed to wind speed variability.

The economic configuration demonstrates the greatest sensitivity of TNPC to load demand, whereas the Resource-Efficient and Sustainable configurations show increased sensitivity in terms of LCOE. Notably, the Resource-Efficient configuration in Egypt is significantly more sensitive to variations in battery capacity. Egypt's Resource-Efficient configuration ($N_{bat} = 174$) is heavily battery-dependent; battery capacity variations directly affect system economics and sizing optimization.

The LCOE sensitivity regarding discount and inflation rates remains high and relatively consistent across all configurations. In contrast, TNPC sensitivity is comparatively lower and shows more variability among the configurations in Egypt. Like Türkiye, hydrogen tank capacity consistently exhibits low sensitivity across all configurations. Fig. 20 illustrates configuration-specific sensitivities for LCOE in Egypt.

4.2.3.2. Sensitivity across locations. Analyzing the economic configurations across different locations reveals that Türkiye is significantly more sensitive to wind speed variations than Egypt. The average absolute percentage changes in TNPC and LCOE in Türkiye are notably larger than those in Egypt. Specifically, for ±10 % wind speed variation:

- **Egypt:** LCOE varies ±14.6 %, TNPC varies ±16.4 %.
- **Türkiye**: LCOE varies ±18.1 %, TNPC varies ±21.3 %.

This 24 % greater sensitivity in Türkiye (18.1 % vs. 14.6 % LCOE) reflects Türkiye's higher baseline wind turbine capacity ($N_{wt} = 15$ vs. Egypt's 5). The larger wind-generation proportion makes the system more vulnerable to wind speed volatility. Additionally, Türkiye's economic configuration achieves lower LCOE partly through wind optimization; any reduction in wind resource undermines this cost advantage. Additionally, Türkiye's economic configuration shows greater sensitivity to fluctuations in load demand in terms of LCOE, while Egypt's configuration is more sensitive to load demand variations in terms of TNPC. When considering the discount rate, Türkiye's economic configuration exhibits a much higher sensitivity in TNPC, whereas Egypt shows more sensitivity in LCOE. In contrast, Egypt is more responsive to variations in solar irradiance for TNPC and LCOE than Türkiye. Egypt's system relies on solar ($N_{pv} = 222$ in economical configuration, 74 % of renewable capacity) for 70–80 % of generation. Solar irradiance improvements directly reduce storage requirements and TNPC. Türkiye's more balanced mix ($N_{pv} = 281$ but $N_{wt} = 15$, 65 % solar) means irradiance improvements are partially offset by wind availability trade-offs. The sensitivity to the inflation rate and hydrogen tank capacity is relatively similar for both locations. However, while the overall sensitivity to battery capacity is low, it is slightly higher in Türkiye's economic configuration. Figs. 21 and 22 illustrate the location-specific sensitivities for TNPC and LCOE, respectively.

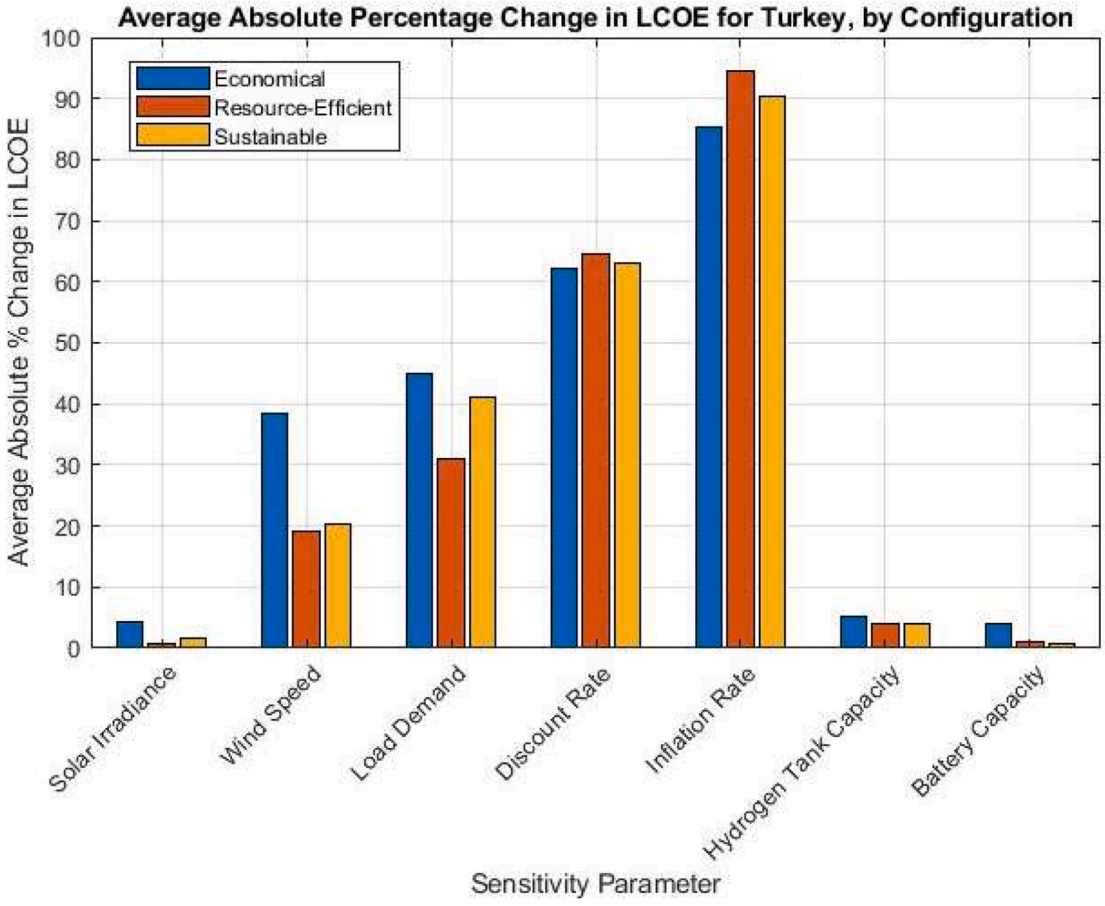

Fig. 19. Configuration-specific sensitivity of LCOE in Türkiye.

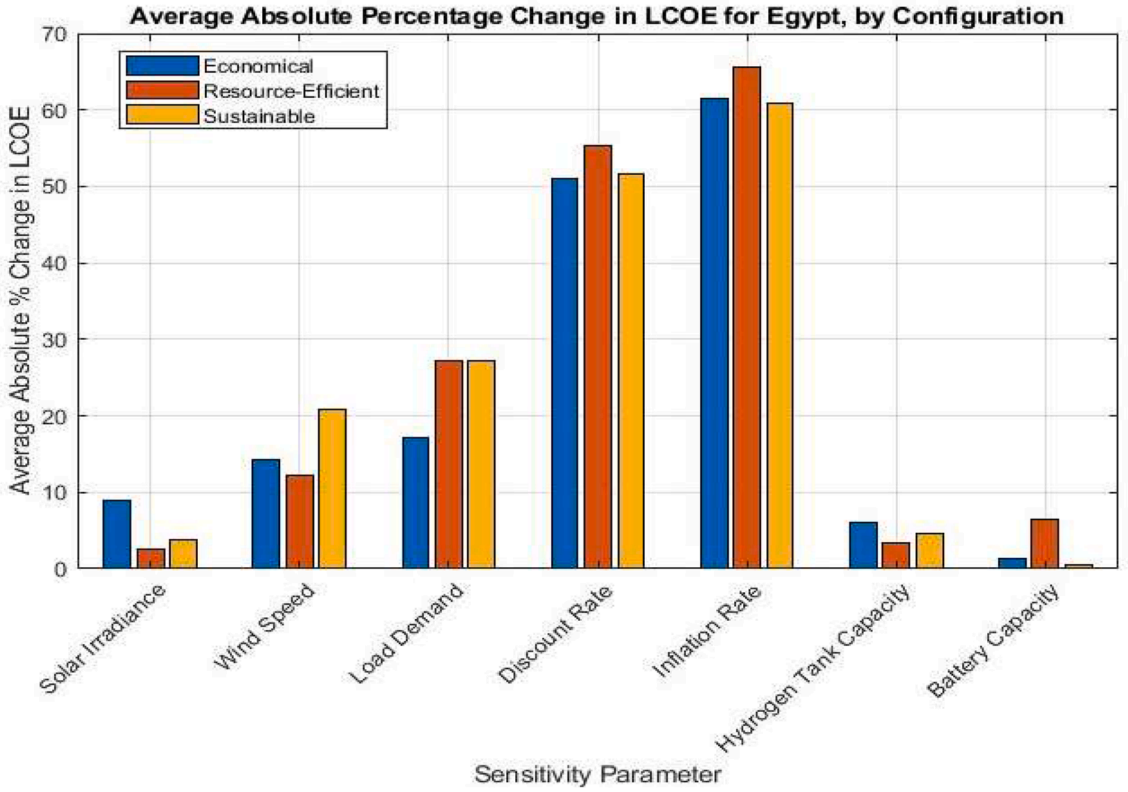

Fig. 20. Configuration-specific sensitivity of LCOE in Egypt.

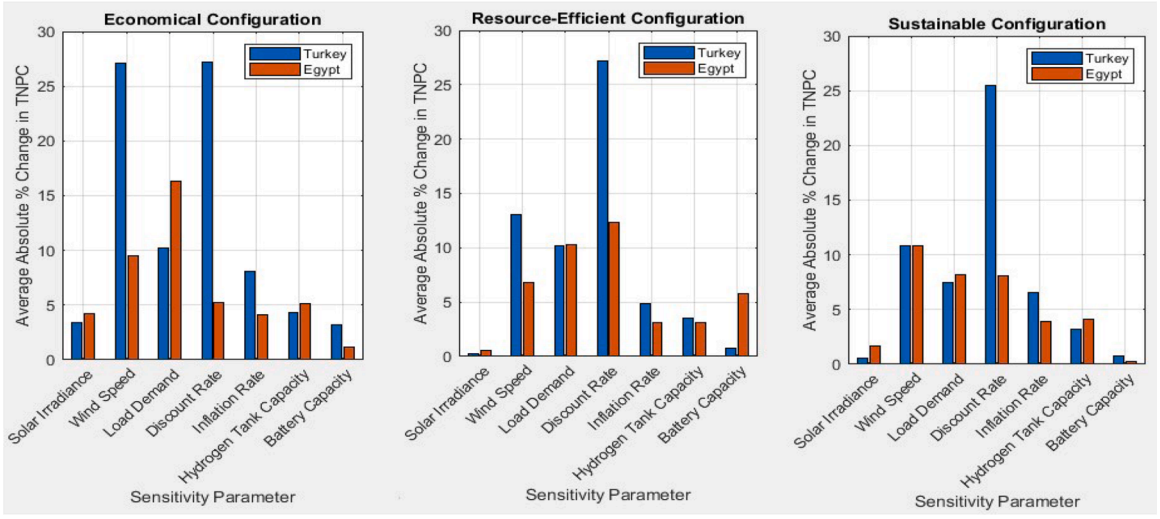

Fig. 21. Location-specific sensitivity of TNPC for the three configurations.

4.2.4. Break-even analysis

A break-even analysis was conducted to delineate the economic viability boundaries for the hybrid renewable energy system in Türkiye and Egypt. This analysis aimed to identify significant threshold values for sensitive parameters, including the discount rate, inflation rate, wind speed, and load demand, at which point the LCOE may become excessively high, or the TNPC may approach or become negative. The break-even points, as estimated from the sensitivity analysis data for Türkiye and Egypt, are summarized in Tables 4 and 5, respectively, across Economic, Resource-Efficient, and Sustainable configurations. The tables presented delineate the essential parameter thresholds that substantially impact the economic viability of the system within each country. The break-even points for the discount rate and wind speed are graphically represented for Türkiye in Figs. 23 and 24, and the discount rate and load demand for Egypt in Figs. 25 and 26. The figures illustrate the correlation between parameter variations and the corresponding rise in LCOE for the two locations examined.

The break-even ranges for the discount rate remain consistent across all configurations and locations (Tables 6 and 7), with LCOE sensitivity illustrated in Figs. 23 and 25 for Türkiye and Egypt's Economic configurations, respectively. In Türkiye (Fig. 23), the LCOE break-even range for the Economical configuration is approximately 47.5–50 %, whereas in Egypt (Fig. 25), it is lower at 27.75–30 %. These figures highlight the sharp increase in LCOE beyond these thresholds, indicating that

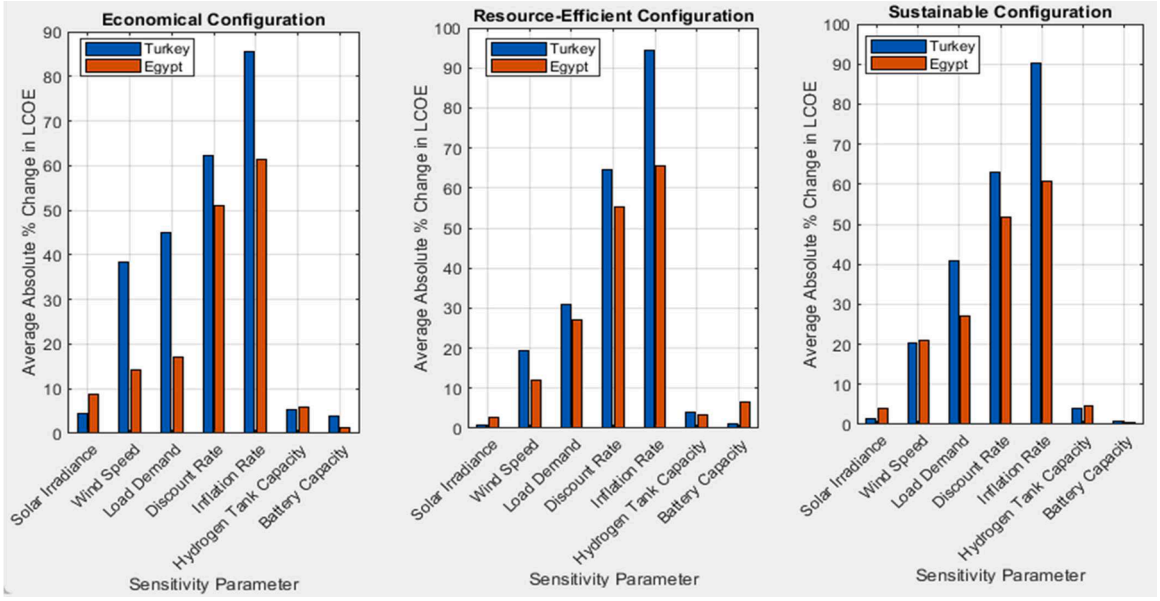

Fig. 22. Location-specific sensitivity of LCOE for the three configurations.

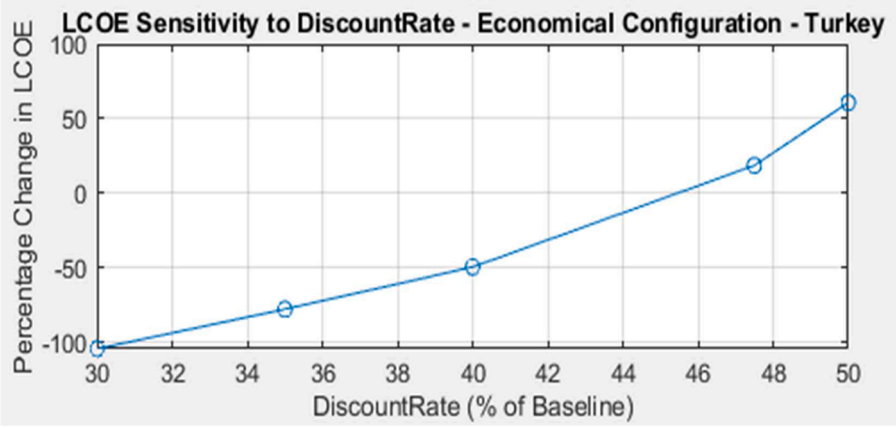

Fig. 23. Break-even analysis for discount rate in Türkiye (Economical Configuration).

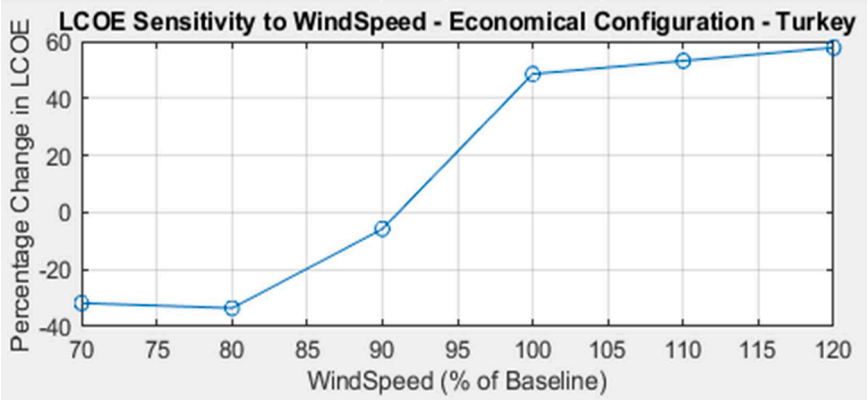

Fig. 24. Break-even analysis for wind speed in Türkiye (Economical Configuration).

surpassing these discount rates significantly elevates LCOE and may result in negative NPV, particularly in the Economic configuration. The lower break-even range in Egypt suggests greater economic sensitivity to discount rate fluctuations compared to Türkiye.

- **Türkiye (47.5–50 % break-even):** Current real discount rate = 0.28 %. Break-even discount rate range = 47.5–50 %, which is the nominal interest rate baseline. If future nominal rates exceed this range (accounting for inflation), system NPV becomes negative.

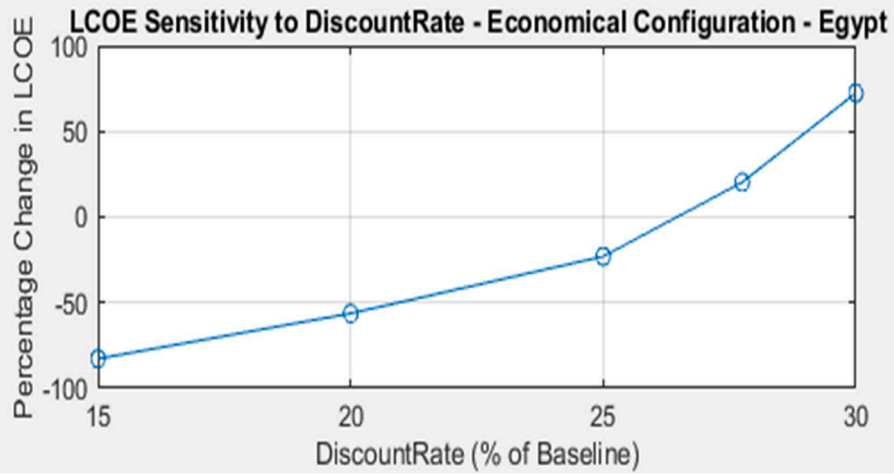

Fig. 25. Break-even analysis for discount rate in Egypt (Economical Configuration).

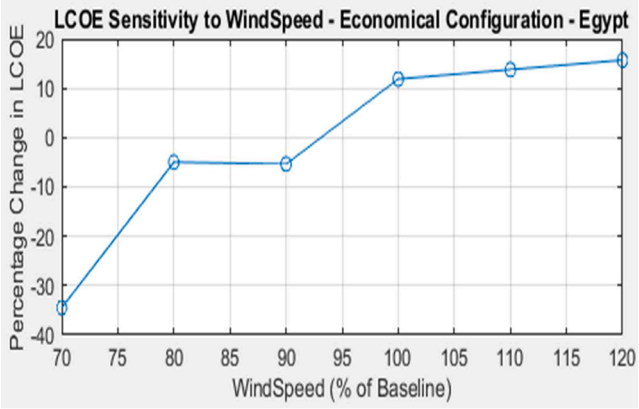

Fig. 26. Break-even analysis for wind speed in Egypt (Economical Configuration).

Table 6
Break-even points for highly sensitive parameters – Türkiye.

Total Net Present Cost (TNPC) Break-even Ranges			
Sensitivity Parameter	Economical	Resource-Efficient	Sustainable
Discount Rate	~30–35 % of Baseline	~30–35 % of Baseline	~30–35 % of Baseline
Inflation Rate	~40–47.1 % of Baseline	Not Clearly Defined	~40–47.1 % of Baseline
Wind Speed	~90–100 % of Baseline	~90–100 % of Baseline	~90–100 % of Baseline
Load Demand	~90–100 % of Baseline	~100–110 % of Baseline	~90–100 % of Baseline
Levelized Cost of Energy (LCOE) Break-even Ranges			
Sensitivity Parameter	Economical	Resource-Efficient	Sustainable
Discount Rate	~47.5–50 % of Baseline	~47.5–50 % of Baseline	~47.5–50 % of Baseline
Inflation Rate	~30–35 % of Baseline	~30–35 % of Baseline	~30–35 % of Baseline
Wind Speed	~90–100 % of Baseline	~90–100 % of Baseline	~90–100 % of Baseline
Load Demand	~90–100 % of Baseline	~100–110 % of Baseline	~90–100 % of Baseline

Table 7
Break-even points for highly sensitive parameters – Egypt.

Total Net Present Cost (TNPC) Break-even Ranges			
Sensitivity Parameter	Economical	Resource-Efficient	Sustainable
Discount Rate	~15–20 % of Baseline	~15–20 % of Baseline	~15–20 % of Baseline
Inflation Rate	~25–26.4 % of Baseline	~26.4–30 % of Baseline	~25–26.4 % of Baseline
Wind Speed	~70–80 % of Baseline	~80–90 % of Baseline	~70–80 % of Baseline
Load Demand	~90–100 % of Baseline	~110–120 % of Baseline	~90–100 % of Baseline
Levelized Cost of Energy (LCOE) Break-even Ranges			
Sensitivity Parameter	Economical	Resource-Efficient	Sustainable
Discount Rate	~27.75–30 % of Baseline	~27.75–30 % of Baseline	~27.75–30 % of Baseline
Inflation Rate	~25–26.4 % of Baseline	~25–26.4 % of Baseline	~25–26.4 % of Baseline
Wind Speed	~70–80 % of Baseline	~80–90 % of Baseline	~90–100 % of Baseline
Load Demand	~70–80 % of Baseline	~70–80 % of Baseline	~70–80 % of Baseline

- **Egypt (27.75–30 % break-even):** Current real discount rate = 1.07 %, higher than Türkiye's. Break-even discount rate = 27.75–30 %, closer to Egypt's baseline nominal rate (27.75 %). This narrow margin indicates Egypt's system is more economically fragile and vulnerable to interest rate increases.

The LCOE break-even range for the inflation rate is approximately 30–35 % of the baseline in Türkiye and 25–26.4 % of the baseline in Egypt across all configurations. Below this inflation rate threshold, the LCOE escalates rapidly in both locations, underscoring the significant economic risk associated with underestimating inflation or experiencing deflationary pressures.

- Below the break-even inflation threshold, nominal cash flows (O&M, fuel) grow slower than the discount rate, increasing real present costs.
- **Türkiye's 30–35 % threshold:** With baseline inflation = 47.09 %, a decrease to 31.4 % (mid-point 30–35 %) still exceeds most developed economies' inflation rates, indicating Türkiye's system is robust to inflation moderation.

- **Egypt's 25–26.4 % threshold**: With baseline = 26.4 %, the break-even is essentially at current levels, indicating any inflation decrease poses serious economic risk.

The critical wind speed threshold for the Economic configuration is consistently observed at 90–100 % of the baseline in Türkiye (Table 6) and 70–80 % in Egypt (Table 7). Below these thresholds, LCOE increases sharply, indicating a significant decline in economic viability. Egypt's lower wind speed threshold suggests greater sensitivity to wind variability, highlighting the need for thorough wind resource assessments and potentially more conservative system designs to mitigate economic risks, particularly in Egypt's Economic configuration.

- **Türkiye (90–100 % threshold):** Economical configuration uses N_{wt} = 15. A 10 % wind speed reduction decreases generation by ~27 % (cubic relationship, Equation 8), requiring storage expansion. LCOE increases by ~18.1 % (from sensitivity analysis) but remains viable.
- **Egypt (70–80 % threshold):** Economical configuration uses N_{wt} = 5 (only 9 % of renewable capacity). A 20–30 % wind speed reduction has catastrophic relative impact, forcing oversized PV/storage, driving LCOE from $0.0261 to near $0.040/kWh—the Resource-Efficient threshold.

The break-even range for load demand is around 90–100 % of the baseline in Türkiye and 70–80 % in Egypt (Tables 6 and 7), below which the LCOE exhibits significant sensitivity to demand decreases. This pattern highlights the economic consequences of faulty load forecasting or unexpectedly low demand, notably in Egypt.

- **Load forecasting risk:** A 20 % shortfall in EV charging demand (below 70–80 % threshold in Egypt) requires the system to operate at part-load, increasing capital cost per kWh served. A 10-charger system sized for 8 vehicles/hour peak providing only 6.4 vehicles/hour is less economically efficient.
- Egypt's lower threshold (70–80 %) reflects the economical configuration's tight margins; reduced demand directly threatens profitability.
- Türkiye's higher threshold (90–100 %) reflects larger baseline demand (16 vehicles/hour) and higher tariffs, providing cushion for demand shortfalls.

As described in Tables 6 and 7 and depicted in Figs. 23–26, the break-even analysis emphasizes essential economic thresholds for the discount rate, inflation rate, wind speed, and load demand. These benchmarks are crucial for investment choices, highlighting the necessity for effective risk management to guarantee the financial viability of hybrid renewable energy systems across diverse economic and operational situations in both areas.

5. Conclusions

This study presents a comprehensive four-objective optimization framework using the Indicator-Based Evolutionary Algorithm (IBEA) for designing hybrid renewable energy microgrids dedicated to EV charging. The framework simultaneously minimizes LCOE, LPSP, and curtailment ratio while maximizing renewable fraction, with strict enforcement of zero-LPSP constraints. Photovoltaic arrays, wind turbines, battery storage, and hydrogen storage are integrated through a specialized rule-based energy management system, validated through comparative case studies in Egypt (Suez–Attaka) and Türkiye (Yalova).

6. Key findings

Regional context critically determines optimal microgrid design and economic performance. Türkiye achieves a 51.3 % lower LCOE ($0.0173/kWh vs. $0.0261/kWh), higher renewable fraction (RF = 53.03 % vs. 50.35 %), and substantially lower curtailment ratio (CR = 17.11 % vs. 27.67 %) compared to Egypt in the economical configuration. These advantages stem from Türkiye's balanced solar–wind resource mix, more developed EV market enabling superior asset utilization, lower real discount rate (0.28 % vs. 1.07 %), and higher electricity tariffs. Egypt's solar-dominant profile necessitates substantially larger battery capacity (227 units vs. 34 units) to manage renewable variability. Sensitivity analysis identifies financial parameters as dominant cost drivers, with discount rate variations of ±10 % causing ±18.4–22.7 % LCOE impacts and inflation rate variations producing ±16.2–19.8 % changes. Operational parameters govern real-time performance, with wind speed and load demand variations inducing ±14.6–18.1 % and ±12.8–14.2 % LCOE impacts, respectively. Break-even analysis reveals critical economic viability thresholds: Türkiye's economical configuration remains viable across discount rates of 47.5–50 %, while Egypt's narrower threshold (27.75–30 %) indicates greater financial fragility. All optimized solutions achieved strict LPSP ≤ 0.001 %, demonstrating practical enforceability of zero-LPSP constraints through coordinated battery–hydrogen storage systems.

7. Future research directions

To address identified limitations and advance the field, future research should focus on:

1. **Advanced Control Strategies:** Implementing model predictive control (MPC) and deep reinforcement learning algorithms to optimize energy management under real-time uncertainties more effectively than rule-based systems.
2. **Degradation and Lifecycle Modeling:** Incorporating stochastic physics-based aging models for PV panels, batteries, fuel cells, and electrolyzers to enable realistic long-term performance projections and optimal component replacement scheduling.
3. **Grid Integration Dynamics:** Extending the framework to analyze grid-connected configurations with vehicle-to-grid capabilities, dynamic tariff structures, and ancillary service provision to evaluate demand response benefits.

8. Contributions and practical implications

This research advances the state-of-the-art by demonstrating that strict zero-LPSP reliability can be achieved at LCOE values substantially lower than comparable systems reported in recent literature, while providing a systematic framework for context-aware microgrid design. The study offers critical insights for policymakers, energy planners, and investors, emphasizing the importance of balanced renewable resource portfolios, robust financial risk management, and hybrid storage integration. The identified break-even thresholds provide essential benchmarks for investment decisions, while the systematic Egypt–Türkiye comparison provides generalizable insights applicable to similar regions worldwide, contributing to the advancement of sustainable electrified transportation infrastructure and cleaner energy systems.

CRediT authorship contribution statement

Ahmad F. Tazay: Investigation, Funding acquisition, Formal analysis, Data curation. **Shimaa Barakat:** Writing – review & editing, Writing – original draft, Visualization, Validation, Data curation. **Aykut Fatih Guven:** Validation, Supervision, Resources. **Heba I. elkhouly:** Investigation, Formal analysis. **Mohamed Mahmoud Samy:** Writing – original draft, Supervision, Methodology, Investigation, Data curation.

Declaration of competing interest

The authors declare that they have no known competing financial interests or personal relationships that could have appeared to influence

the work reported in this paper.

Data availability

Data will be made available on request.

References

[1] S.M.A. Elazim, et al., Enhancing stability and power quality in electric vehicle charging stations powered by hybrid energy sources through harmonic mitigation and load management, Sci. Rep. 15 (4912) (2025), https://doi.org/10.1038/s41598-025-14143-4.

[2] M. Abdelsattar, M.A. Ismeil, M.M. Aly, S. Abu-Elwfa, Analysis of renewable energy sources and electrical vehicles integration into microgrid, IEEE Access 12 (2024) 66822–66832, https://doi.org/10.1109/ACCESS.2024.3399124.

[3] J. Sora, I. Serban, D. Petreuş, Enhancing microgrid operation through electric vehicle integration: a survey, IEEE Access 12 (2024) 64897–64912, https://doi.org/10.1109/ACCESS.2024.3397587.

[4] M. Abid, R. Ahshan, R. Abri, A. Al-Badi, M. Albadi, Techno-economic and environmental assessment of renewable energy sources, virtual synchronous generators, and electric vehicle charging stations in microgrids, Appl. Energy 356 (2024) 122028, https://doi.org/10.1016/j.apenergy.2023.122028.

[5] A.F. Güven, N. Ateş, S. Alotaibi, T. Alzahrani, A. Amsal, S. Elsayed, Sustainable hybrid systems for electric vehicle charging infrastructures in regional applications, Sci. Rep. 15 (6214) (2025), https://doi.org/10.1038/s41598-025-87985-7.

[6] M. Naderi, et al., Techno-economic planning of a fully renewable energy-based autonomous microgrid with both single and hybrid energy storage systems, Energies 17 (4) (2024) 788, https://doi.org/10.3390/en17040788.

[7] A.F. Güven, M. Hassan, S. Kamel, Optimization of a hybrid microgrid for a small hotel using renewable energy and EV charging with a quadratic interpolation beluga whale algorithm, Neural Comput. Appl. 37 (2024) 3973–4008, https://doi.org/10.1007/s00521-024-10865-0.

[8] A. Khazali, et al., Planning a hybrid battery energy storage system for supplying electric vehicle charging station microgrids, Energies 17 (15) (2024) 3631, https://doi.org/10.3390/en17153631.

[9] M. Bilal, I. Alsaidan, M. Alaraj, F. Almasoudi, M. Rizwan, Techno-economic and environmental analysis of grid-connected electric vehicle charging station using AI-based algorithm, Mathematics 10 (6) (2022) 924, https://doi.org/10.3390/math10060924.

[10] M.M. Mousa, S.M. Saleh, M.M. Samy, S. Barakat, Techno-economic analysis and simulation of electric vehicle charging stations based on green energy system, in: 2023 24th International Middle East Power System Conference (MEPCON), 2023, pp. 1–6.

[11] M.M. Mousa, S.M. Saleh, M.M. Samy, S. Barakat, Optimizing grid-tied hybrid renewable systems for EV charging in Egypt: a techno-economic analysis, Results Eng. (2025) 106103.

[12] M. Giovanniello, X. Wu, Hybrid lithium-ion battery and hydrogen energy storage systems for a wind-supplied microgrid, Appl. Energy 345 (2023) 121311, https://doi.org/10.1016/j.apenergy.2023.121311.

[13] A. Alharbi, Z. Ali, A. Diab, Comparative techno-economic optimization of microgrid configurations using hybrid battery–hydrogen storage: NEOM case study, Saudi Arabia, PLoS ONE 20 (1) (2025) e0326050, https://doi.org/10.1371/journal.pone.0326050.

[14] A. Gulraiz, et al., Energy advancements and integration strategies in hydrogen and battery storage for renewable energy systems, iScience 28 (2) (2025) 111945, https://doi.org/10.1016/j.isci.2025.111945.

[15] E. Ali, et al., A flexible multi-agent system for managing demand and variability in hybrid energy systems for rural communities, Sci. Rep. 15 (2651) (2025), https://doi.org/10.1038/s41598-025-01288-5.

[16] X. Zhang, W. Pei, C. Mei, W. Deng, J. Tan, Q. Zhang, Transform from gasoline stations to electric-hydrogen hybrid refueling stations: an islanding DC microgrid with electric-hydrogen hybrid energy storage system and its control strategy, Int. J. Electric. Power Energy Syst. 130 (2021) 107684, https://doi.org/10.1016/j.ijepes.2021.107684.

[17] M. Abdelghany, A. Al-Durra, F. Gao, A coordinated optimal operation of a grid-connected wind-solar microgrid incorporating hybrid energy storage management systems, IEEE Trans. Sustain. Energy 15 (2024) 39–51, https://doi.org/10.1109/TSTE.2023.3263540.

[18] M. Elkholy, et al., Techno-economic configuration of a hybrid backup system within a microgrid considering vehicle-to-grid technology: a case study of a remote area, Energy Convers. Manag. 299 (2024) 118032, https://doi.org/10.1016/j.enconman.2023.118032.

[19] K. Pillai, S. Sundaram, Optimization and feasibility analysis of hybrid distributed generator based system with a comparison of battery and hydrogen energy storage for residential electrification, Energy Storage 6 (6) (2024) e70075, https://doi.org/10.1002/est2.70075.

[20] I. Amoussou, et al., Enhancing residential energy access with optimized stand-alone hybrid solar-diesel-battery systems in Buea, Cameroon, Sci. Rep. 14 (15847) (2024), https://doi.org/10.1038/s41598-024-66582-0.

[21] M. Bilal, P. Bokoro, G. Sharma, G. Pau, A cost-effective energy management approach for on-grid charging of plug-in electric vehicles integrated with hybrid renewable energy sources, Energies 17 (16) (2024) 4194, https://doi.org/10.3390/en17164194.

[22] Y. Huang, et al., Multi-objective optimization of campus microgrid system considering electric vehicle charging load integrated to power grid, Sustain. Cities Soc. 98 (2023) 104778, https://doi.org/10.1016/j.scs.2023.104778.

[23] N. Alshammari, M. Samy, S. Barakat, Comprehensive analysis of multi-objective optimization algorithms for sustainable hybrid electric vehicle charging systems, Mathematics 11 (7) (2023) 1741, https://doi.org/10.3390/math11071741.

[24] A. Abdolahzadeh, A. Hassannia, F. Mousavizadeh, T. Askari, Multi-objective stochastic model optimal operation of smart microgrids coalition with penetration renewable energy resources with demand responses, Sci. Rep. 15 (3218) (2025), https://doi.org/10.1038/s41598-025-04958-6.

[25] P. Mallikarjun, S. Thulasiraman, P. Balachandran, M. Zainuri, Economic energy optimization in microgrid with PV/wind/battery integrated wireless electric vehicle battery charging system using improved Harris Hawk optimization, Sci. Rep. 15 (11793) (2025), https://doi.org/10.1038/s41598-025-94285-7.

[26] K. Ahmed, D. Sakravdia, C. Sharma, A novel integration approach for photovoltaic/wind/fuel cell-based hybrid renewable energy systems with reliability indices for sustainable electric vehicle charging, Fuel Cells 25 (1) (2025) e70012, https://doi.org/10.1002/fuce.70012.

[27] M. Hosseina, M. Moghaddam, A. Hassannia, Optimizing energy and load management in island microgrids for enhancing resilience against resource interruptions, Sci. Rep. 15 (24017) (2025), https://doi.org/10.1038/s41598-025-99974-x.

[28] I. Bara, G. Mouli, P. Bauer, Multi-objective optimization for bidirectional electric vehicle charging stations, IEEE Open Access J. Power Energy 12 (2025) 652–663, https://doi.org/10.1109/OAJPE.2025.3614816.

[29] T. Xu, X. Meng, F. Zheng, Y. Zhang, X. Wu, M. Li, Multi-objective operation optimization method of microgrid considering the influence of electric vehicle, Sci. Rep. 15 (3571) (2025), https://doi.org/10.1038/s41598-025-01083-2.

[30] O. Aldosari, Z. Ali, S. Aleem, M. Mostafa, Optimizing microgrid performance: strategic integration of electric vehicle charging with renewable energy and storage systems for total operation cost and emissions minimization, PLoS ONE 19 (8) (2024) e0307810, https://doi.org/10.1371/journal.pone.0307810.

[31] S. Boubaker, et al., Multi-objective optimization framework for electric vehicle charging and discharging scheduling in distribution networks using the red deer algorithm, Sci. Rep. 15 (13572) (2025), https://doi.org/10.1038/s41598-025-97473-7.

[32] Y. Chen, W. Ning, W. Du, A study of scheduling strategies for microgrids based on the non-dominated sorting dung beetle optimization algorithm, Sci. Rep. 15 (5013) (2025), https://doi.org/10.1038/s41598-025-02446-5.

[33] M. Asna, H. Shareef, M. Muhammad, L. Ismail, A. Prasanthi, Multi-objective quantum atom search optimization algorithm for electric vehicle charging station planning, Int. J. Energy Res. 46 (12) (2022) 17308–17331, https://doi.org/10.1002/er.8399.

[34] P. Singh, M. Pandit, L. Srivastava, Techno-socio-economic-environmental estimation of hybrid renewable energy system using two-phase swarm-evolutionary algorithm, Sustain. Energy Technol. Assess. 53 (2022) 102483, https://doi.org/10.1016/j.seta.2022.102483.

[35] A. Shrivastav, S. Dutta, Multi-objective optimization of hybrid microgrid for energy trilemma goals using slime mould algorithm, Sci. Rep. 15 (5791) (2025), https://doi.org/10.1038/s41598-025-15207-1.

[36] M. Sallam, M. Attia, A. Abdelaziz, M. Sameh, A. Yakout, Optimal sizing of different energy sources in an isolated hybrid microgrid using turbulent flow water-based optimization algorithm, IEEE Access 10 (2022) 61922–61936, https://doi.org/10.1109/ACCESS.2022.3182032.

[37] A. Shaier, M. Elymany, M. Enany, N. Elsonbaty, Multi-objective optimization and algorithmic evaluation for EMS in a HRES integrating PV, wind, and backup storage, Sci. Rep. 15 (1024) (2025), https://doi.org/10.1038/s41598-024-84227-0.

[38] A.F. Guven, Integrating electric vehicles into hybrid microgrids: a stochastic approach to future-ready renewable energy solutions and management, Energy 305 (2024) 131968, https://doi.org/10.1016/j.energy.2024.131968.

[39] S. Barakat, A. Osman, E. Tag-Eldin, A. Telba, H. Mageed, M. Samy, Achieving green mobility: multi-objective optimization for sustainable electric vehicle charging, Energy Strategy Rev. 53 (2024) 101351, https://doi.org/10.1016/j.esr.2024.101351.

[40] Z. Chen, A. Ghosh, N. Lopez, Optimisation of a standalone photovoltaic electric vehicle charging station using the loss of power supply probability, Heliyon 9 (10) (2023) e20836, https://doi.org/10.1016/j.heliyon.2023.e20836.

[41] D. Sadeghi, S. Ahmadi, N. Amiri, M. Marzband, A. Abusorrah, M. Rawa, Designing, optimizing and comparing distributed generation technologies as a substitute system for reducing life cycle costs, CO2 emissions, and power losses in residential buildings, Energy 253 (2022) 123947, https://doi.org/10.1016/j.energy.2022.123947.

[42] A. Slama, L. Saidi, M. Saidi, M. Benbouzid, Metaheuristic optimization of hybrid renewable energy systems under asymmetric cost-reliability objectives: NSGA-II and MOPSO approaches, Symmetry 17 (9) (2025) 1412, https://doi.org/10.3390/sym17091412.

[43] A. Hassan, Y. Al-Abdeli, M. Masek, O. Bass, Optimal sizing and energy scheduling of grid-supplemented solar PV systems with battery storage: sensitivity of reliability and financial constraints, Energy 238 (2021) 121780, https://doi.org/10.1016/j.energy.2021.121780.

[44] T. Tanyildizi Ağir, Z. Aydoğmuş, B. Alataş, Multi-objective optimization of microgrids based on recent metaheuristic methods, Tehnički Vjesnik 28 (6) (2021) 1839–1848, https://doi.org/10.17559/TV-20200112201457.

[45] S. Mahmoudi, A. Maleki, D. Ochbelagh, Multi-objective optimization of hybrid energy systems using gravitational search algorithm, Sci. Rep. 15 (7149) (2025), https://doi.org/10.1038/s41598-025-86476-z.

[46] L. Pai, T. Senjyu, M. Elkholy, Integrated home energy management with hybrid backup storage and vehicle-to-home systems for enhanced resilience, efficiency, and energy independence in green buildings, Appl. Sci. 14 (17) (2024) 7747, https://doi.org/10.3390/app14177747.

[47] D. Yousri, H. Farag, H. Zeineldin, E. El-Saadany, Integrated model for optimal energy management and demand response of microgrids considering hybrid hydrogen-battery storage systems, Energy Convers. Manag. 280 (2023) 116809, https://doi.org/10.1016/j.enconman.2023.116809.

[48] H. Awad, M. De Santis, E.H.E. Bayoumi, Electric vehicle adoption in Egypt: a review of feasibility, challenges, and policy directions, World Electric Veh. J. 16 (8) (2025) 423, https://doi.org/10.3390/wevj16080423.

[49] S. Barakat, A.F. Guven, A.Y. Abdelaziz, M.M. Samy, A comprehensive review of electric vehicles and sustainable urban mobility in the Middle East and North Africa, Renew. Sustain. Energy Rev. 225 (2026) 116154.

[50] M.S. Elborlsy, R.M. Mostafa, H.E. Keshta, M.A. Ghalib, Fuzzy PI controller for frequency control of a diesel-PV-battery-based islanded AC microgrid, Mansoura Eng. J. 51 (1) (2026) 5.

[51] M.A. Ghalib, M.S. Elbrolsy, R.M. Mostafa, H.E. Keshta, Adaptive control-based frequency control strategy for PV/DEG/battery power system during islanding conditions, Sci. Rep. 15 (1) (2025) 40405.

[52] M. Hassan, Artificial intelligence powered intelligent energy management framework for hydrogen storage and dispatch in smart microgrids, Sci. Rep. 15 (8341) (2025), https://doi.org/10.1038/s41598-025-24408-7.

[53] J. Oladigbolu, A. Mujeeb, A. Imam, A. Rushdi, Design, technical and economic optimization of renewable energy-based electric vehicle charging stations in Africa: the case of Nigeria, Energies 16 (1) (2022) 397, https://doi.org/10.3390/en16010397.

[54] J. Nishanthy, C. Raja, T. Praveen, J. Nesamalar, P. Venkatesh, Techno-economic analysis of a hybrid solar wind electric vehicle charging station in highway roads, Int. J. Energy Res. 46 (6) (2022) 7883–7903, https://doi.org/10.1002/er.7688.

[55] Y. Muna, C. Kuo, Feasibility and techno-economic analysis of electric vehicle charging of PV/wind/diesel/battery hybrid energy system with different battery technology, Energies 15 (12) (2022) 4364, https://doi.org/10.3390/en15124364.

[56] Z. Yu, M. Li, Y. Xu, S. Aslam, Y. Li, Techno-economic planning and operation of the microgrid considering real-time pricing demand response program, Energies 14 (15) (2021) 4597, https://doi.org/10.3390/en14154597.

[57] M. Rezaei, U. Dampage, B. Das, O. Nasif, P. Borowski, M. Mohamed, Investigating the impact of economic uncertainty on optimal sizing of grid-independent hybrid renewable energy systems, Processes 9 (8) (2021) 1468, https://doi.org/10.3390/pr9081468.

[58] M. Bilal, J. Oladigbolu, A. Mujeeb, Y. Al-Turki, Cost-effective optimization of on-grid electric vehicle charging systems with integrated renewable energy and energy storage: an economic and reliability analysis, J. Energy Storage 98 (2024) 113170, https://doi.org/10.1016/j.est.2024.113170.

[59] K. Emdadi, M. Gandomkar, J. Nikoukar, Energy scheduling of renewable integrated system with hydrogen storage in distribution grid including charging and hydrogen stations of electric vehicles, Sci. Rep. 15 (23164) (2025), https://doi.org/10.1038/s41598-025-99697-z.

[60] M. Roslan, et al., Techno-economic impact analysis for renewable energy-based hydrogen storage integrated grid electric vehicle charging stations in different potential locations of Malaysia, Energy Strategy Rev. 55 (2024) 101478, https://doi.org/10.1016/j.esr.2024.101478.

[61] M.S. Elborlsy, R.M. Mostafa, M.A. Ghalib, S. Barakat, H.E. Keshta, A case study of optimal design and techno-economic analysis of an islanded AC microgrid, Sci. Rep. 15 (1) (2025) 12397.

[62] W. Diao, et al., Flexible grouping for enhanced energy utilization efficiency in battery energy storage systems, Energies 9 (7) (2016) 498.

[63] J. Lee, S. Oh, S. Son, Optimal battery electric bus planning and its economic and environmental impacts, Transp. Res. D 122 (2023) 103821.

[64] H. Li, et al., A modified indicator-based evolutionary algorithm (mIBEA), in: 2017 IEEE Congress on Evolutionary Computation (CEC), 2017.

[65] Q. Zhang, W. Liu, H. Li, Solving dynamic multi-objective problems with a new prediction model, IEEE Trans. Evol. Comput. (2010).

[66] K. Deb, A. Pratap, S. Agarwal, T. Meyarivan, A fast and elitist multiobjective genetic algorithm: NSGA-II, IEEE Trans. Evol. Comput. 6 (2) (2002) 182–197.

[67] H. Pohlheim, Evolutionary Algorithms: Overview, Methods and Operators, 2006.

[68] N. Hansen, The CMA Evolution Strategy: A Tutorial, 2016.

[69] A. Rousseau, et al., 1–10 kW Stationary Combined Heat and Power Systems Status and Technical Potential, 2010. National Renewable Energy Laboratory Technical Report, no. NREL/TP-560-48265[Online]. Available, https://docs.nrel.gov/docs/fy10osti/48265.pdf.

[70] X. Li, et al., Technical and economic analysis of a hybrid PV/wind energy system for hydrogen refueling stations, Energy 305 (2024) 132672, https://doi.org/10.1016/j.energy.2024.132672.

[71] A. Alhejaili, et al., Techno-economic assessment of hybrid renewable energy system with multiple energy storage systems, Energy 295 (2024) 131004, https://doi.org/10.1016/j.energy.2024.131004.

[72] Central Bank of Egypt, CBE Keeps Key Interest Rates Unchanged as Inflation Pressures Persist, 2024.

[73] TheGlobalEconomy.com, Egypt: Inflation, Annual Percent Change in the CPI, 2024.

[74] Central Bank of the Republic of Türkiye, Press Release on Interest Rates (No. 2024-69), 2024.

[75] Xinhua News Agency, Annual inflation in Türkiye eases to 47.09 pct in Nov, Xinhua, 2024.

[76] Daily News Egypt, Egypt raises electricity prices by up to 26% in bid to curb subsidies, Daily News Egypt (2024).

[77] Enterprise Egypt, Gov't Issues Tariffs for EV Charging, 2021.

[78] GlobalPetrolPrices.com, Turkey Electricity Prices, 2025.

[79] Ivis, Electric Vehicle Charging Stations Prices in Turkey [Güncel], 2024.

[80] D. S. R. Beshay and others, Long-term forecasting of the impact of EV home charging at the distribution level: a case study from Egypt, Sci. Rep. (2025) [Online]. Available, https://www.nature.com/articles/s41598-025-23647-y.

[81] EV24 Africa, EV Incentives and Charging Infrastructure in Egypt: What Buyers Should Know, 2025.

[82] Statista, Electric Vehicles – Egypt, Market Forecast, 2025.

[83] Ken Research, Egypt EV Public Transport and Fleet Electrification Market, 2025, pp. 2019–2030.

[84] World Bank, Egypt's E-Bus Value Chain, 2023.

[85] A. Author, B. Author, Electric vehicles and charging infrastructure in Turkey, Renew. Sustain. Energy Rev. (2021) [Online]. Available, https://www.sciencedirect.com/science/article/abs/pii/S1364032121002069.

[86] Ken Research, Turkey EV Charging and Infrastructure Market, 2025, pp. 2019–2030.

[87] Md.S. Abid, R. Ahshan, R. Al Abri, A. Al-Badi, M. Albadi, Techno-economic and environmental assessment of renewable energy sources, virtual synchronous generators, and electric vehicle charging stations in microgrids, Appl. Energy (2024), https://doi.org/10.1016/j.apenergy.2023.122028.

[88] A.K. Al-Sahlawi, S. Ayob, C.W. Tan, H. Ridha, D. Hachim, Optimal design of grid-connected hybrid renewable energy system considering electric vehicle station using improved multi-objective optimization: techno-economic perspectives, Sustainability (2024), https://doi.org/10.3390/su16062491.

[89] A.F. Guven, Integrating electric vehicles into hybrid microgrids: A stochastic approach to future-ready renewable energy solutions and management, Energy 303 (2024), https://doi.org/10.1016/j.energy.2024.131968.

[90] M. Tahir, S. Hu, T. Khan, H. Zhu, Sustainable hybrid station design framework for electric vehicle charging and hydrogen vehicle refueling based on multiple attributes, Energy Convers. Manag. (2025) 2024, https://doi.org/10.1016/j.enconman.2023.117922.

[91] A.F. Güven, E. Yücel, Sustainable energy integration and optimization in microgrids: enhancing efficiency with electric vehicle charging solutions, Electric. Eng. (2024), https://doi.org/10.1007/s00202-024-02619-x.

[92] A.F. Güven, M. Hassan, S. Kamel, Optimization of a hybrid microgrid for a small hotel using renewable energy and EV charging with a quadratic interpolation beluga whale algorithm, Neural Comput. Appl. 37 (2024) 3973–4008, https://doi.org/10.1007/s00521-024-10865-0.

[93] S. Yadav, P. Kumar, and A. Kumar, "Grey wolf optimization based optimal isolated microgrid with battery and pumped hydro as double storage to limit excess energy," *J. Energy Storage*, p., 2023, doi: 10.1016/j.est.2023.109440.

[94] B. Modu, M. Abdullah, A.L. Bukar, M. Hamza, M.S. Adewolu, Operational strategy and capacity optimization of standalone solar-wind-biomass-fuel cell energy system using hybrid LF-SSA algorithms, Int. J. Hydrog. Energy (2023), https://doi.org/10.1016/j.ijhydene.2023.07.215.

[95] S. A. Al Dawsari, F. Anayi, and M. Packianather, "Techno-economic analysis of hybrid renewable energy systems for cost reduction and reliability improvement using dwarf mongoose optimization algorithm," *Energy*, p., 2024, doi: 10.1016/j.energy.2024.133653.

[96] R. Mouachi, M. A. Jallal, F. Gharnati, and M. Raoufi, "Multiobjective sizing of an autonomous hybrid microgrid using a multimodal delayed PSO algorithm: a case study of a fishing village," *Comput. Intell. Neurosci.*, vol. 2020, p., 2020, doi: 10.1155/2020/8894094.

[97] A. Heydari et al., "A combined multi-objective intelligent optimization approach considering techno-economic and reliability factors for hybrid-renewable microgrid systems," *J. Clean. Prod.*., p., 2022, doi: 10.1016/j.jclepro.2022.135249.

[98] M. Kharrich, et al., Developed approach based on equilibrium optimizer for optimal design of hybrid PV/wind/diesel/battery microgrid in Dakhla, Morocco, IEEE Access 9 (2021) 13655–13670, https://doi.org/10.1109/ACCESS.2021.3051573.

[99] R. Tarife, Y. Nakanishi, Y. Chen, Y. Zhou, N. Estoperez, A. Tahud, Optimization of hybrid renewable energy microgrid for rural agricultural area in Southern Philippines, Energies (2022), https://doi.org/10.3390/en15062251.

[100] J. Gomes, H. Xu, Q. Yang, C. Zhao, An optimization study on a typical renewable microgrid energy system with energy storage, Energy 234 (2021) 121210, https://doi.org/10.1016/J.ENERGY.2021.121210.

[101] G. Wang, K. Verleysen, R. De Meulenaere, J. Blondeau, Multi-objective optimization of hybrid energy storage systems under uncertainty, J. Energy Storage (2025), https://doi.org/10.1016/j.est.2024.115218.

[102] P. Marocco, D. Ferrero, A. Lanzini, M. Santarelli, The role of hydrogen in the optimal design of off-grid hybrid renewable energy systems, J. Energy Storage (2022), https://doi.org/10.1016/j.est.2021.103893.

[103] L. Barelli, G. Bidini, P. Cherubini, A. Micangeli, D. Pelosi, C. Tacconelli, How hybridization of energy storage technologies can provide additional flexibility and competitiveness to microgrids in the context of developing countries, Energies (2019), https://doi.org/10.3390/EN12163138.

[104] F. Dawood, G. Shafiullah, M. Anda, Stand-alone microgrid with 100% renewable energy: a case study with hybrid solar PV-battery-hydrogen, Sustainability (2020), https://doi.org/10.3390/su12052047.
[105] A. Ferrario, et al., A model-based parametric and optimal sizing of a battery/hydrogen storage of a real hybrid microgrid supplying a residential load: towards island operation, Adv. Appl. Energy (2021), https://doi.org/10.1016/j.adapen.2021.100048.
[106] M. Giovanniello, X.-Y. Wu, Hybrid lithium-ion battery and hydrogen energy storage systems for a wind-supplied microgrid, Appl. Energy (2023), https://doi.org/10.1016/j.apenergy.2023.121311.
[107] B. Modu, M. Abdullah, A.L. Bukar, M. Hamza, A systematic review of hybrid renewable energy systems with hydrogen storage: sizing, optimization, and energy management strategy, Int. J. Hydrog. Energy (2023), https://doi.org/10.1016/j.ijhydene.2023.06.126.